3/51

V-20-81
8-31-82

IITRI
IIT Research Institute

(NASA-CR-169716) CREEP-RUPTURE BEHAVIOR OF IRON SUPERALLOYS IN HIGH PRESSURE HYDROGEN Quarterly Narrative Report, 1 Oct. - 31 Dec. 1980 (IIT Research Inst.) 81 p
HC A05/MF A01

N83-15410

Unclas
CSCL 11F G3/26 01976

Report No. IITRI-M6061-15

CREEP-RUPTURE BEHAVIOR OF IRON SUPERALLOYS IN HIGH-PRESSURE HYDROGEN

NASA-Lewis Research Center
Cleveland, Ohio 44135

Attention: Mr. Robert H. Titran
Project Manager
Materials Development Center
Materials and Structures Division

Prepared by

S. Bhattacharyya

IIT Research Institute
10 West 35 Street
Chicago, Illinois 60616

20 January 1981

Fifth Quarterly Narrative Report Covering
Period 1 October to 31 December 1980

FOREWORD

This quarterly report summarizes the work done during 1 October to 31 December 1980 on NASA Project, "Creep-Rupture Behavior of Iron Superalloys in High-Pressure Hydrogen." The report is given the IITRI designation, IITRI-M6061-15.

During this quarter additional air-creep rupture tests were completed bringing the total to 143 tests. In addition, 22 tests are under way. It is expected that all air-creep tests will be completed during the next quarter. In this report, an extensive analysis of existing data is summarized.

The high-pressure H_2 creep-rupture facility was assembled during this period. All NASA test specimens were H_2 charged and sent to NASA immediately. During December, various calibration tests were conducted using high pressure H_2. It is expected that after doing some more trial tests during January 1981, initial rupture tests will be initiated in late February 1981.

Air-creep tests were conducted by H. Nichols. Many people contributed to the H_2 test equipment development, and of them the following have made significant contributions: J. Lamoureux, C. Hales, J. Mok, R. Katos, E. Vesely, and W. Peterman.

The report was edited by V. Johnson and typed by P. Sullivan.

S. Bhattacharyya
Senior Engineer

Maurice A. H. Howes, Director
Materials & Manufacturing Technology

TABLE OF CONTENTS

LIST OF TABLES

LIST OF FIGURES

LIST OF FIGURES (cont.)

CREEP-RUPTURE BEHAVIOR OF IRON SUPERALLOYS IN HIGH-PRESSURE HYDROGEN

1. INTRODUCTION

The objective of this program is to evaluate the creep-rupture properties of six candidate iron-base high-temperature alloys for use as constructional materials in the Stirling engine. The creep-rupture behavior of these alloys at temperatures of 650° to 925°C (1200° to 1700°F) will be determined in air for 10 to 3000 hr, and in 20.7 MPa (3000 psi) H_2 for 10 to 300 hr. The resulting data will be analyzed to determine the effect of high-pressure H_2 on the properties and microstructures of these alloys.

2. TECHNICAL PROGRAM

The project was initiated on 27 September 1979, and consists of the following five tasks:

- Task I - Materials Procurement, Preparation, and Air Testing
- Task II - High-Pressure Hydrogen Testing
- Task III - Data Analysis
- Task IV - Hydrogen Charging
- Task V - Reporting Requirements.

During the period 1 October to 31 December 1980, the following activities were performed:

2.1 Task I - Material Procurement, Preparation, and Air Testing

2.1.1 Specimen Preparation

Six iron-base alloys--A-286, Incoloy 800H, N-155, 19-9DL, CRM-6D, and XF-818--are under evaluation. Of these six, CRM-6D and XF-818 are cast alloys and the other four are sheet alloys in the thickness range of 0.79 to 0.99 mm (0.031 to 0.039 in.). The cast alloy specimens were cast by Climax Molybdenum Company of Ann Arbor, and a copy of Climax Report CP-211, entitled

"Preparation of CRM-6D and XF-818 Threaded Test Bars by Investment Casting," hasbeen sent to NASA separately.

In Fig. 1, typical as-cast and machined specimens as well as investment molds are shown. The nominal chemical analyses of the six alloys and the heat analyses of the two cast alloys are given in Table 1. The cast specimens have a gage diameter of 6.35 mm (0.250 in.) for air testing and 3.96 mm (0.156 in.) for H_2 testing. All the cast specimens were radiographed, and those with no flaws are being tested.

The sheet alloy specimens for H_2 testing were reinforced at the pin-loading holes by laser welding pieces of the same material across it. Typical specimens are shown in Fig. 2. Figure 2b shows the weld bead on A-286 formed at 25.4 mm/s (60 ipm) with a 2.5 kJ/s power and a spot size of 1 mm. All the materials were given the heat treatment as outlined in Table 2 after all machining and welding were completed.

2.1.2 Air Creep-Tupture Testing

A total of 143 tests have been completed and 22 more are under testing. The stress level and temperature of the tests-in-progress are summarized in Table 3. All the completed test data are given in Section 2.3.

2.2 Task II - High-pressure Hydrogen Testing

2.2.1 General Description

A detailed description of the high-pressure hydrogen testing equipment was given in the last quarterly report (IITRI-M6061-12). This special test facility has been developed for the creep-rupture evaluation of materials in up to 20.7 MPa hydrogen at up to 925°C. Six specimens can be tested simultaneously within a single vessel. A central support column holds the specimens along with extensometers, thermocouples, and strain gages (Fig.3). The entire assembly is lowered into the pressure vessel, which is mounted on a vibration damping frame to avoid specimen interactions (Fig.4).

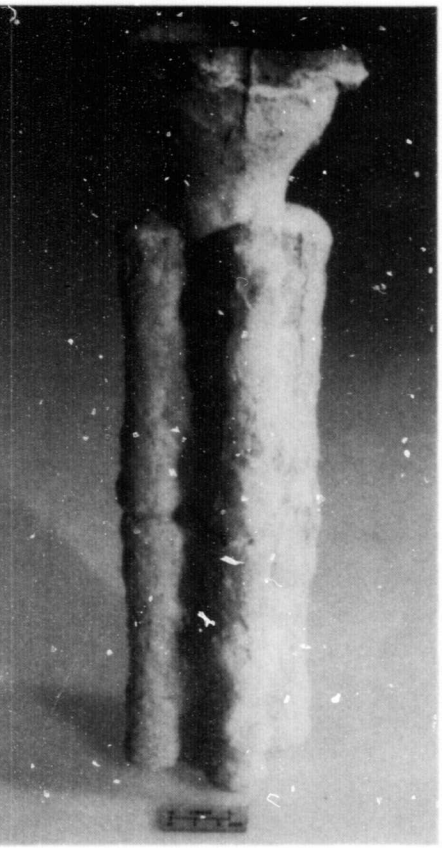

(a)

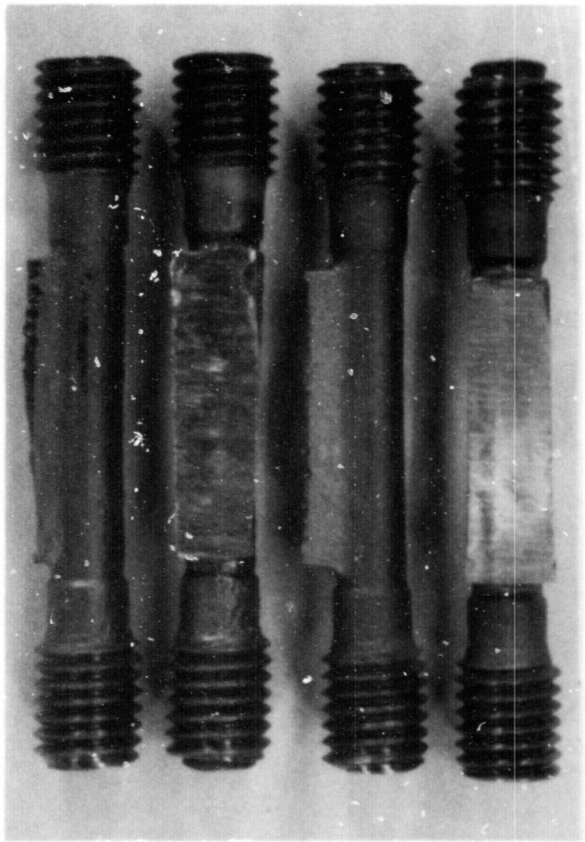

Neg. No. 52269 1-1/8X

(b)

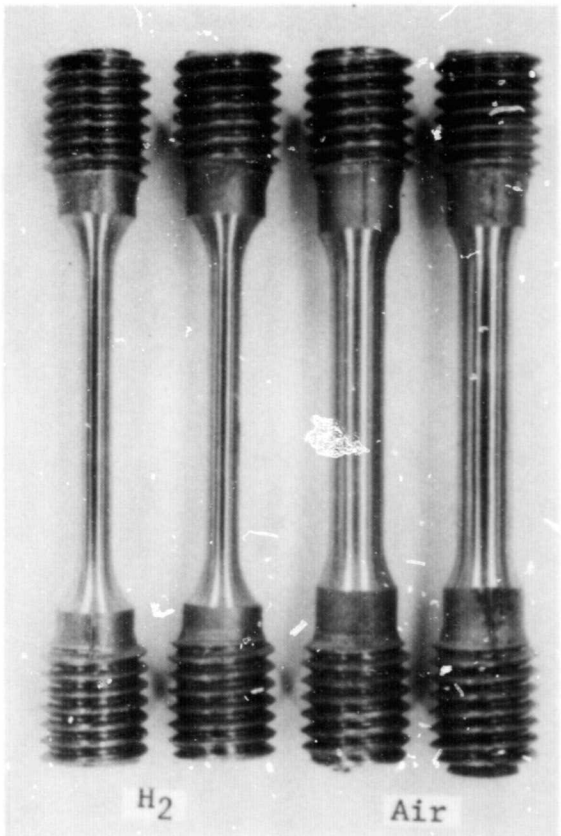

Neg. No. 52518 1X

(c)

Figure 1

Cast Specimen Mold Design and As-Cast Appearance.
(a) Two-tier, four-in-a-tier design with gate feeding into the gage section. (b) As-cast specimen with excess gate material removed from the gage section.
(c) Machined specimens for H_2 and air.

Table 1

NOMINAL CHEMICAL COMPOSITION OF IRON-BASE ALLOYS

Alloys	Nominal Composition, %													
	C	Mn	Si	Cr	Ni	Co	Mo	W	Cb	Ti	Al	B	Fe	Others
A-286	0.05	1.40	0.40	15	26	-	1.25	-	-	2.15	0.2	0.003	Bal	0.03 V
Incoloy 800H	0.05	0.8	0.5	21	32.5	-	-	-	-	0.4	0.4	-	46	0.4 Cu
N-155	0.15	1.5	0.5	21	20	20	3.0	2.5	1.0	-	-	-	Bal	0.15 N
19-9DL	0.30	1.10	0.60	19	9.0	-	1.25	1.20	0.40	0.30	-	-	Bal	-
CRM-6D[a]	1.05	5.00	0.50	22	5.0	-	1.0	1.0	1.0	-	-	0.003	Bal	-
XF-818[a]	0.20	0.15	0.30	18	18	-	7.5	-	0.40	-	-	0.70	Bal	0.12 N
[a] Heat analyses of cast specimens. Sample No. 6365 (CRM-6D) and No. 6366 (EX-818).														
CRM-6D	1.08	4.65	0.46	22.9	5.56	-	0.98	0.98	0.97	-	-	0.007	Bal	0.069 N 0.008 P 0.013 S
XF-818	0.21	0.29	0.34	18.3	18.0	-	7.32	-	0.43	-	-	0.75	Bal	0.106 N 0.007 P 0.010 S

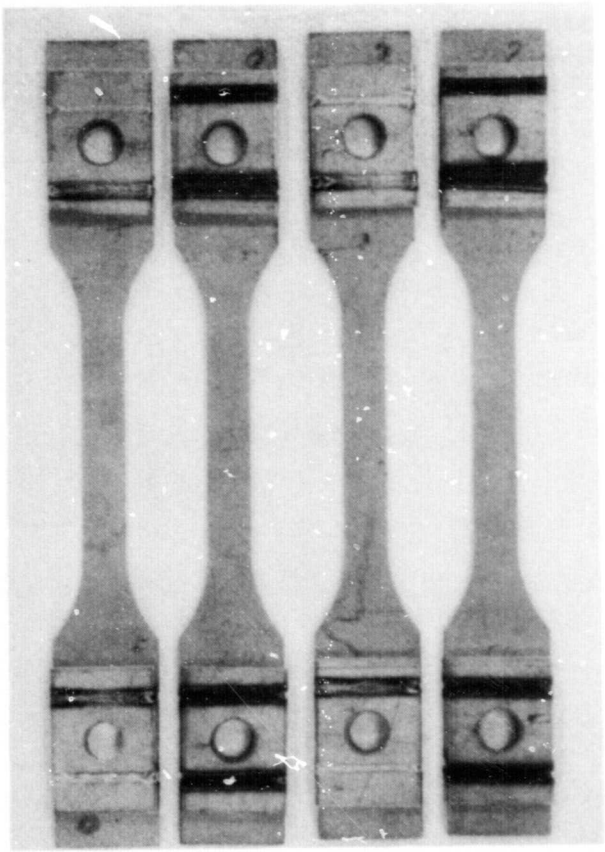

Neg. No. 52514 1X

(a)

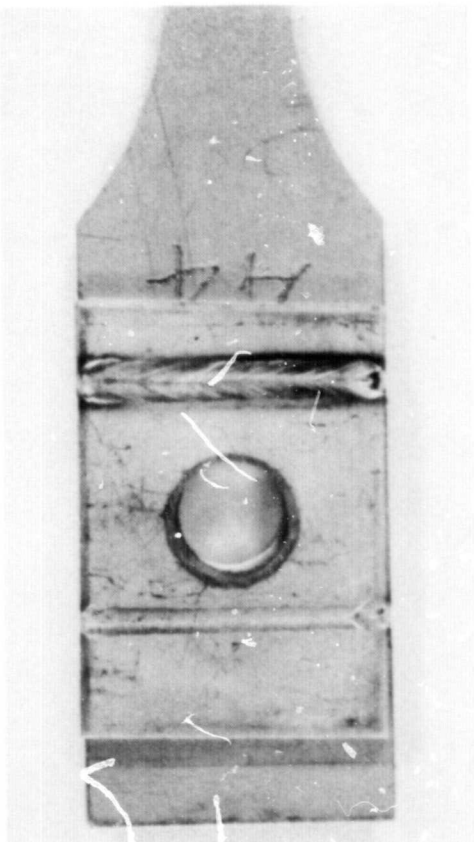

Neg. No. 52516 2.5X

(b)

Figure 2

Sheet Specimens for H_2 Testing with Laser-Welded Reinforcements
(a) Location of welds with respect to pin holes;
(b) details of weld bead.

Table 2

ALLOY SPECIFICATIONS AND HEAT TREATMENT CONDITION FOR TEST SPECIMENS

Alloy	Specification	Heat Treatment (in vacuum)
A-286	5525D[a]	Solution 2100°F[b,c] Age 1325°F-16 hr/AC
Incoloy 800H	5871D[d]	Solution 2100°F[b,c]
N-155	5532C[e] or 5585B[f]	Solution 2150°F[b,c]
19-9DL	5526E[g]	Solution 2200°F-10 min[c]
CRM-6D	(None available)	Age 1200°F-100 hr
XF-818	(None available)	None specified

[a]AMS 5525D revised 10/15/79 supersedes AMS 5525C.
[b]Solution annealing time of 1 hr/in. thickness minimum.
[c]Rapid cool or quench from solution temperature.
[d]AMS 5871D issued 5/15/72.
[e]AMS 5532C revised 7/15/77 supersedes AMS 5532B.
[f]AMS 5585B revised 1/15/78 supersedes AMS 5585A.
[g]AMS 5526E revised 1/15/78 supersedes AMS 5526D.

Table 3

AIR CREEP-RUPTURE TESTS IN PROGRESS

Alloy	Test Temp., °C	Stress, MPa
A-286	760	207
	870	31
Incoloy 800H	815	52
	870	26
	870	34
N-155	705	159
	760	97
	870	47
19-9DL	650	310
	870	29
CRM-6D	650	393
	705	255
	815	131
	870	97
	870	138
	870	172
	925	103
XF-818	650	393
	705	283
	815	103
	815	117
	925	55

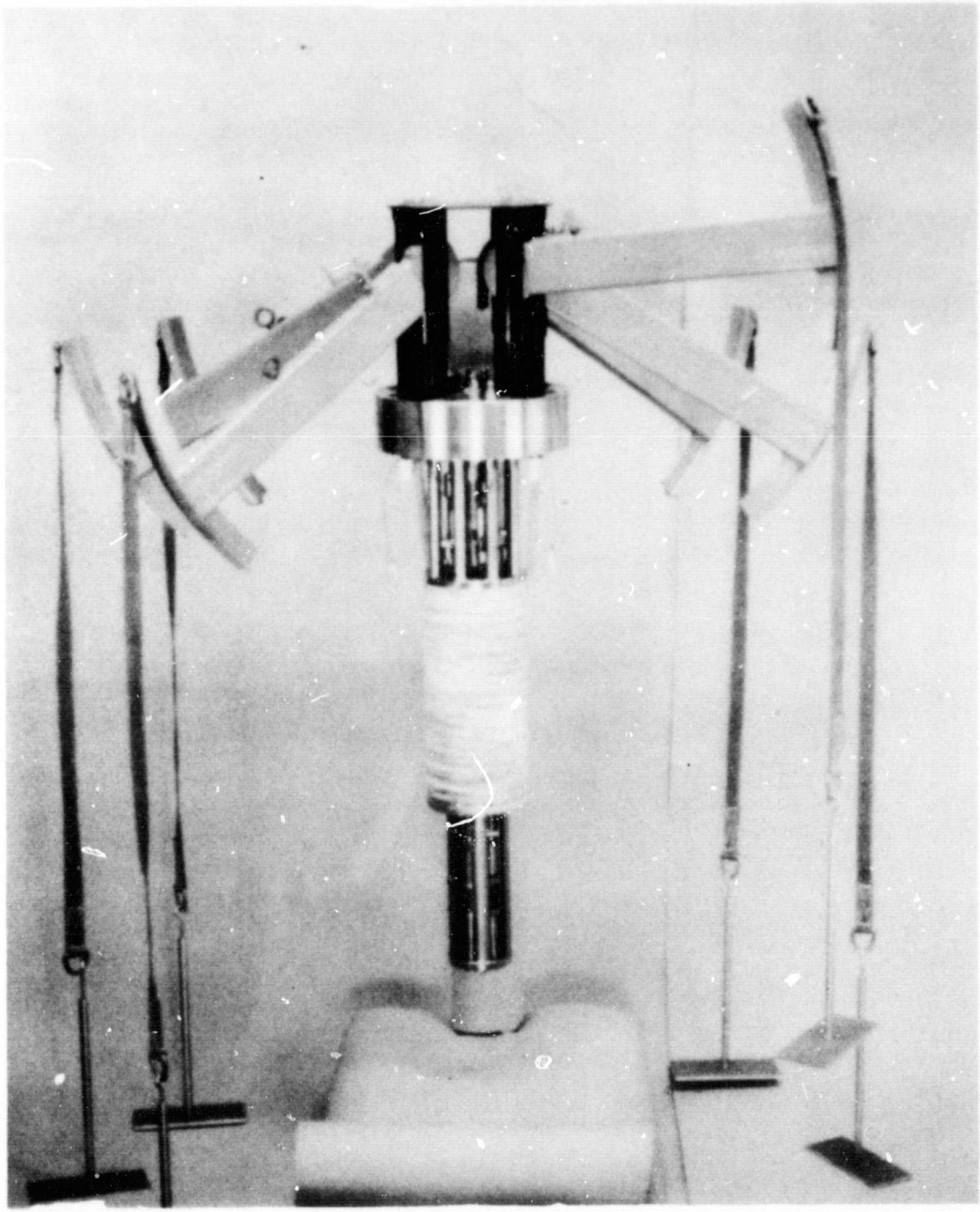

Figure 3

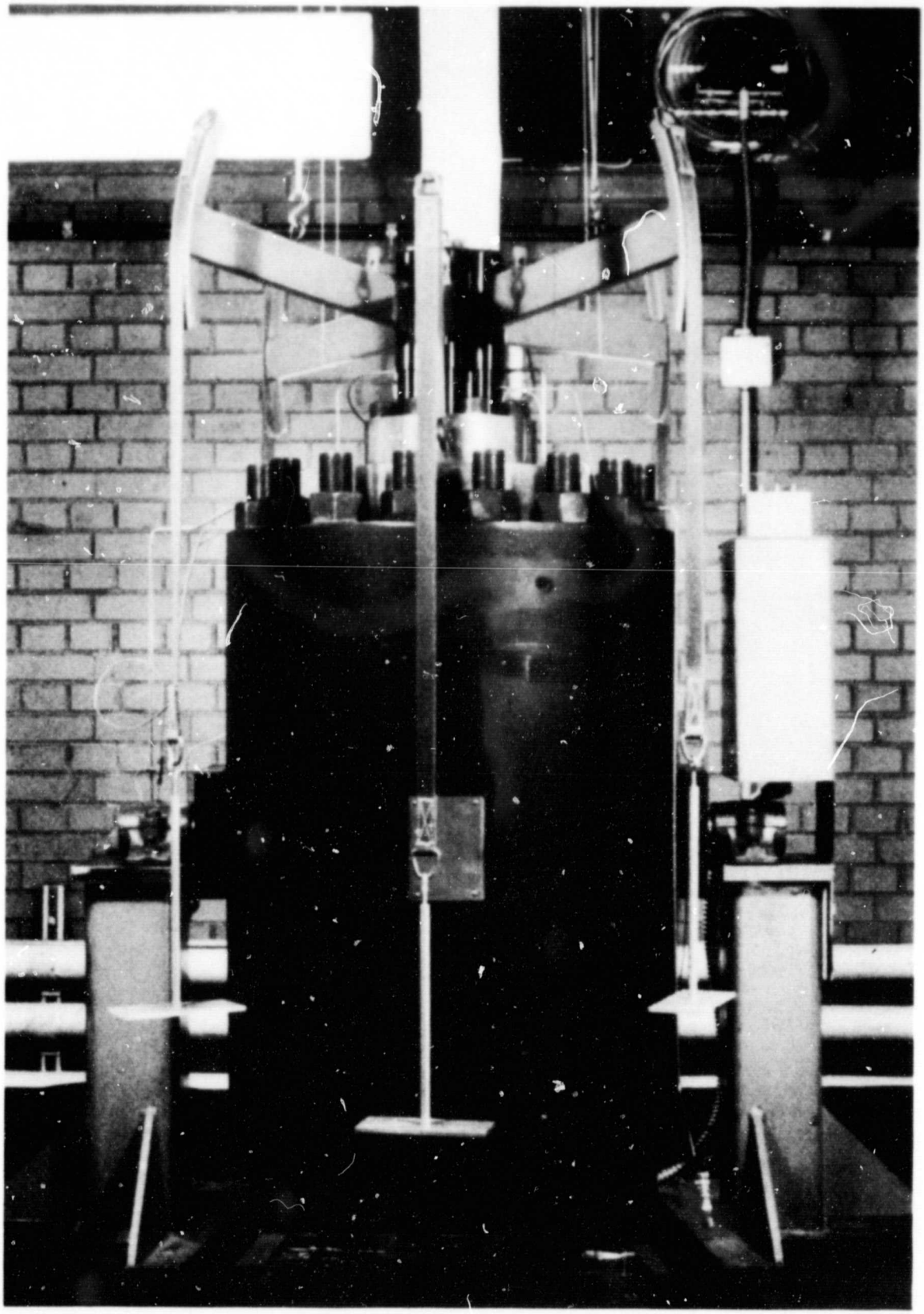

Figure 4

Pressure Vessel with Support Column and Specimens Mounted Inside

The complex apparatus may be grouped into three sections for discussion of the current status. These are:

- Structural and building modification
- Creep vessel system
- Control system

2.2.2 Structural and Building Modifications

The testing facility is located in the northeast corner of the Materials Technology Building on the first floor (Fig. 5). All building modifications have been completed. These include installation of a 2-ton crane, a steel enclosure, a blow-out window, and an explosion-proof ventilation fan.

2.2.3 Creep Vessel System

The pressure vessel has been checked out at temperature and pressure. Some leaks were encountered in start-up, and there were initial difficulties in maintaining a small enough differential pressure between the reactor (H_2) and the jacket (N_2). These problems were resolved, and the system now operates satisfactorily. Hydrogen charging of NASA specimens was completed during the last quarter.

Assembly of the central support column has been completed, and six specimens with thermocouples have been mounted on the column. It will be installed, and the vessel will be brought up to temperature and pressure, in order that a temperature profile for the entire reactor can be plotted. After sufficient temperature stability has been ensured, preparations will be made for preliminary high-pressure creep tests in hydrogen, using dummy specimens.

2.2.4 Control System

The control system was checked out, and a few minor problems were encountered and corrected. The system worked well during the hydrogen charging experiments, and no future problems are foreseen.

Figure 5

View of the Test Chamber with the Pressure Vessel Inside
and the Control Panel and Data Logger Outside

The data acquisition system has been logging data from the air creep experiments conducted in the basement floor, and has had no problems. The data logger has been programmed to accept data from the high-pressure tests and is ready to scan these channels. Data will be recorded both by a printer for hard copies, and by a floppy disk unit for computer analysis.

2.3 Task III - Data Analysis

All the basic creep-rupture data are summarized in Appendix A for the six different alloys. In addition to the basic data, detailed information on time to reach elongation levels of 0.1, 1.0, and 5.0% and the tertiary creep stage are also summarized in Appendix A.

For a clear understanding of the analysis that follows, certain terminologies used in the analysis are identified with the help of a schematic of a creep elongation vs. time curve, shown in Fig. 6. On loading, there is an extension at essentially zero time, the extent of which depends on load and temperature. Creep elongation of the specimen continues with time usually divided into three stages, as shown in Fig. 6. In the secondary stage, the creep rate usually reaches a minimum value called the minimum creep rate ($\dot{\varepsilon}_m$). The duration of the secondary stage gets smaller with increasing load and/or temperature.

At the end of the secondary stage, the creep rate starts to increase and the time at which this occurs is called the time to tertiary creep (t_{ter}). At some time beyond t_{ter}, rupture takes place and the total time is called rupture life (t_r). The difference between t_r and t_{ter} is called the residual tertiary stage life ($t_r - t_{ter}$), where the specimen may elongate significantly depending on its property and environment.

While a few of the air-creep tests are still in progress, there are sufficient data for a meaningful graphical and statistical analysis. The analyses performed during this quarter are summarized in Table 4.

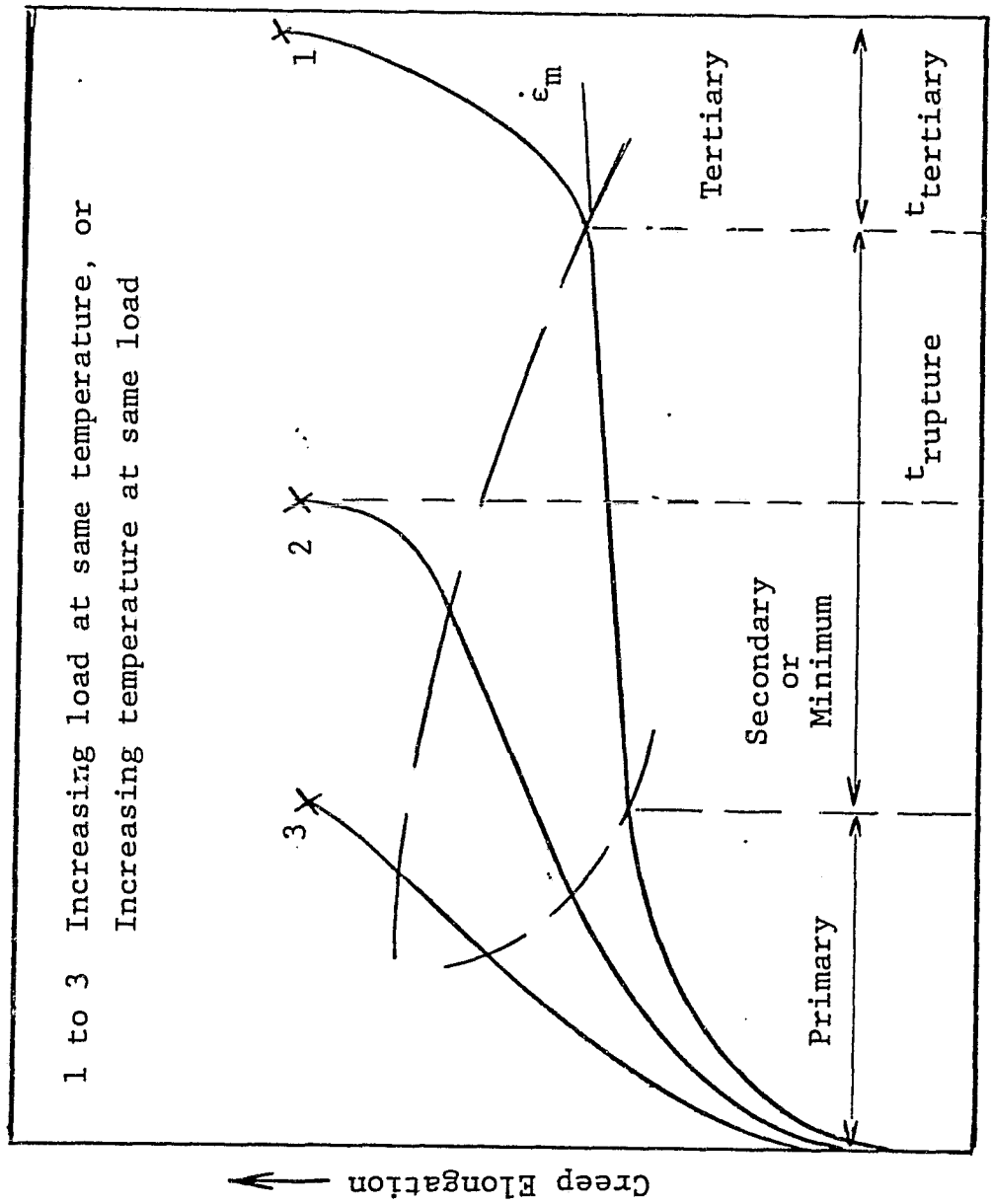

Figure 6

A Schematic Creep Elongaton vs. Time Curve in Iron-Base Alloys at Temperatures Exceeding 0.4 T_m

Table 4

ANALYSIS OF AIR CREEP-RUPTURE DATA

A. Statistical Analysis of 19-9DL Data

Fig. 4	Stress (σ) vs. Time to Rupture (t_r)
Fig. 5	Stress (σ) vs. Time to 1% Creep Elongation ($t_{0.01}$)
Fig. 6	Stress (σ) vs. Time to Tertiary Creep (t_{ter})
Fig. 7	Stress (σ) vs. Residual Tertiary Stage Life ($t_r - t_{ter}$)
Fig. 8	Stress (σ) vs. Total Elongation (ε_t)
Fig. 9	Stress (σ) vs. Minimum Creep Rate ($\dot{\varepsilon}_m$)
Fig. 10	Rupture Life vs. Time to 1% Creep Elongation ($t_{0.01}$)
Fig. 11	Min. Creep Rate vs. Time to 1% Creep Elongation ($t_{0.01}$)
Fig. 12	Residual Tertiary Stage Life vs. Total Elongation (ε_t)
Table 5 Fig. 13	Temperature-Compensated Rupture Life vs. Stress
Table 6	Temperature-Compensated Analysis of Minimum Creep Rate Data

B. Statistical Analysis of Rupture Life Data for Different Alloys

Fig. 14	Stress vs. Rupture Life (t_r), A-286
Fig. 15	Stress vs. Rupture Life (t_r), IN 800H
Fig. 16	Stress vs. Rupture Life (t_r), N-155
Fig. 17	Stress vs. Rupture Life (t_r), CRM-6D
Fig. 18	Stress vs. Rupture Life (t_r), XF-818

C. Variation of Stress-Life Exponent with Temperature in Six Different Alloys

Fig. 19

Table 7

D. Temperature-Compensated Statistical Analysis of Rupture Life

Table 8	Alloy N-155
Table 9	Alloy XF-818

2.3.1 Statistical Analysis of 19-9DL Data

The rupture life data given in Table A-4 are plotted vs. stress in Fig. 7. Statistically fitted lines were drawn at each temperature except for 650°C where only 2 data were available. The lines were not all parallel indicating an effect of temperature on the simple relationship as shown below:

$$t_r = a\sigma^n$$

or

$$\ln t_r = \ln a + n \ln \sigma \qquad (1)$$

where n is the stress exponent or line slope and a is a constant. The correlation coefficients (R^2) for these lines ranged from 0.96 to >0.99.

For comparison, NASA data[1] were plotted on Fig. 4 and indicated a good fit with the IITRI data.

In Fig. 8, time to 1% creep elongation ($t_{0.01}$) was plotted against stress and showed a relationship similar to that observed for t_r vs. σ.

The relationship between stress and t_{ter}, shown in Fig. 9, indicated a trend similar to that in Figs. 7 and 8, but with slightly more scatter. These lines were given an estimated fit and were not fitted statistically to the data points. In particular, one 815°C and another 870°C data showed more deviation at relatively high stress levels where low rupture lives were observed. Exclusion of high stress test and low rupture life data were studied in detail and are reported later in this section.

Finally, in Fig. 10, stress was correlated with residual tertiary stage life ($t_r - t_{ter}$). Again, these lines were given

---

[1] Walter R. Witske and Joseph R. Stephens, "Creep Rupture Behavior of Seven Iron-Base Alloys After Long Term Aging at 760°C in Low Pressure Hydrogen," NASA TM-81534, August 1980, NASA-Lewis Research Center, Cleveland, Ohio.

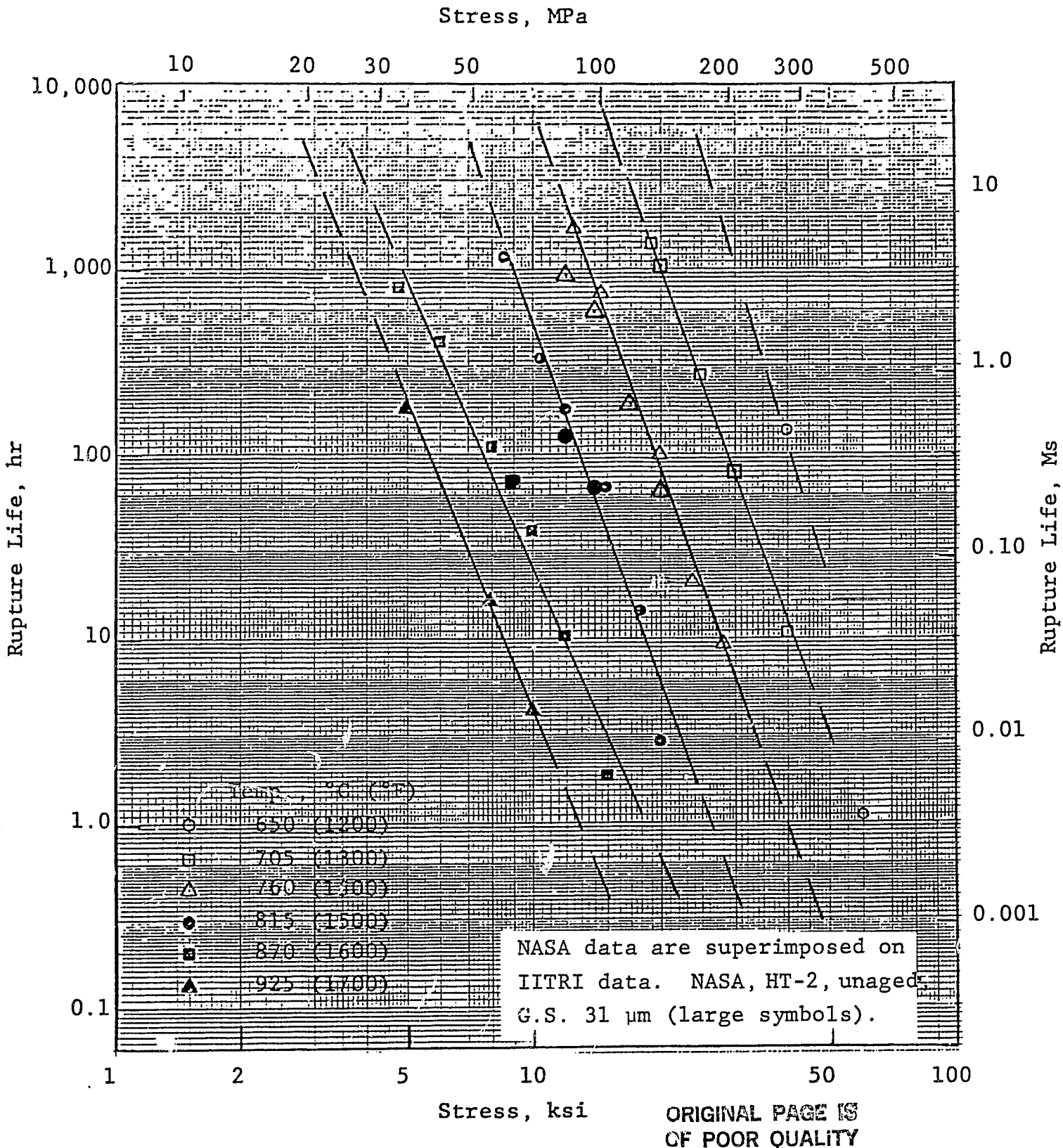

ORIGINAL PAGE IS
OF POOR QUALITY

Figure 7

Stress vs. Rupture Life, 19-9DL, Unaged (G.S. 33 μm)--
A Comparison of IITRI and NASA Data

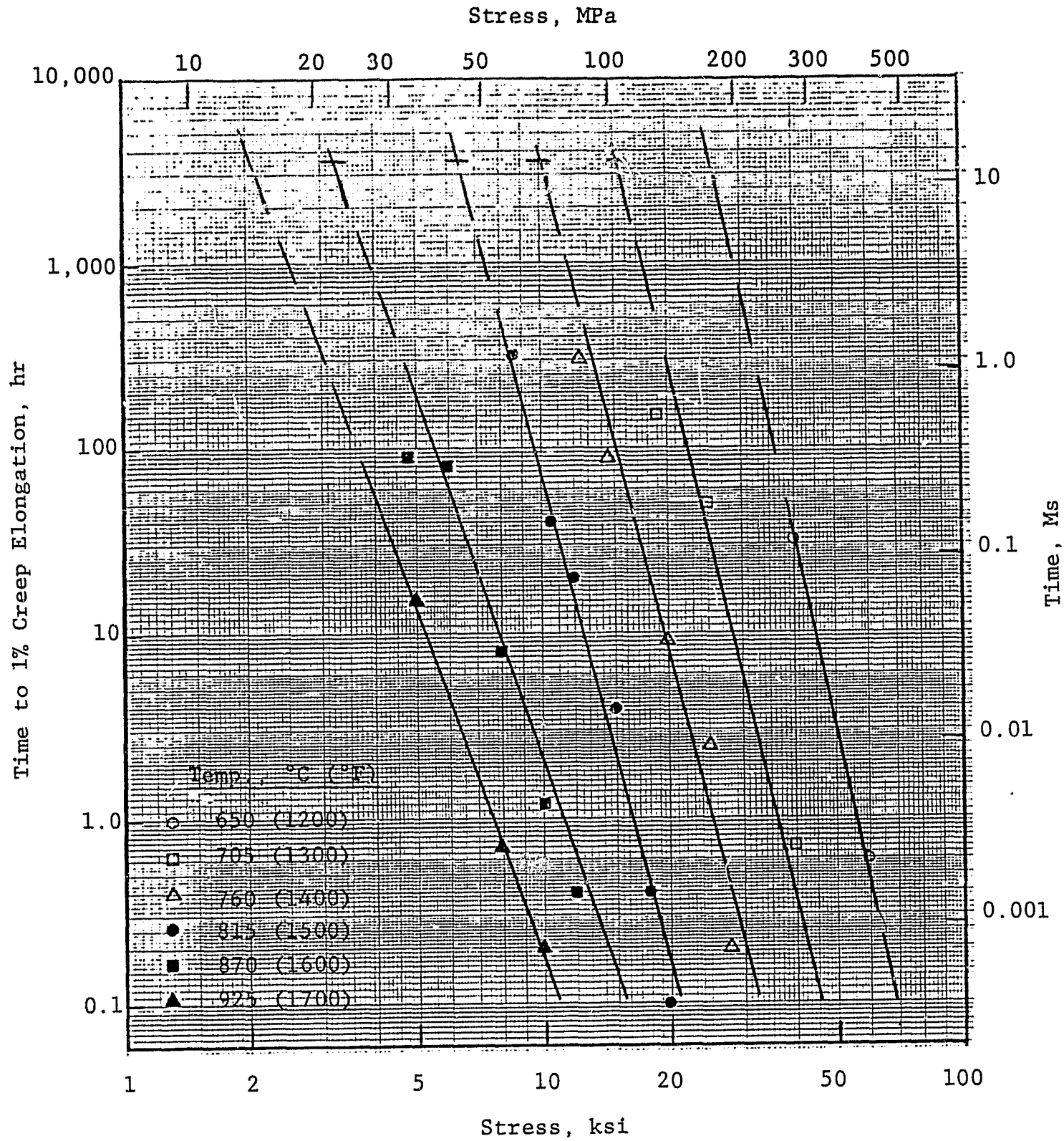

Figure 8

Stress vs. Time to 1% Creep Elongation,
19-9DL, Unaged (G.S. 33 μm)

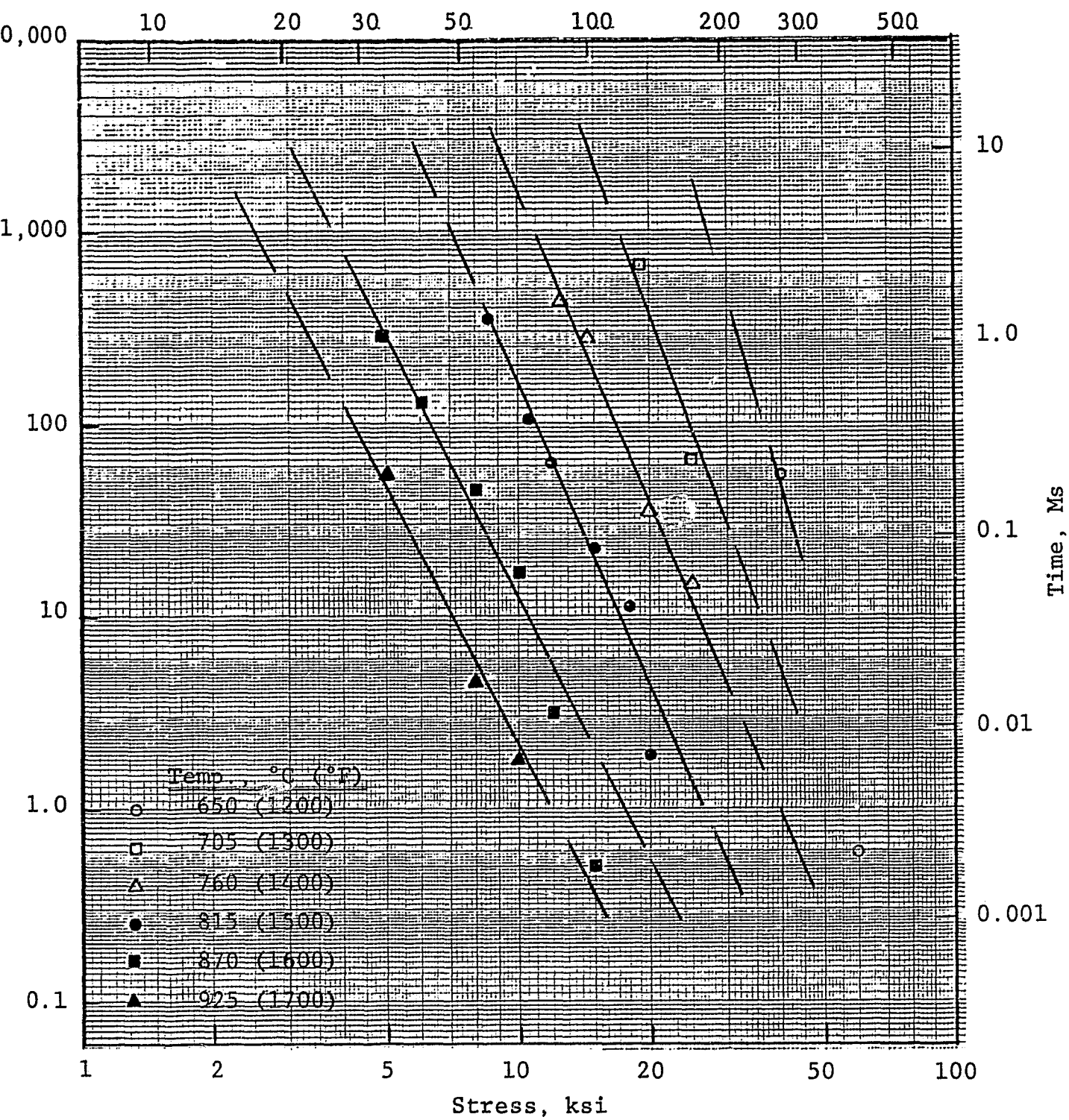

Figure 9

Stress vs. Time to Reach Tertiary Stage,
19-9DL, Unaged (G.S. 33 μm)

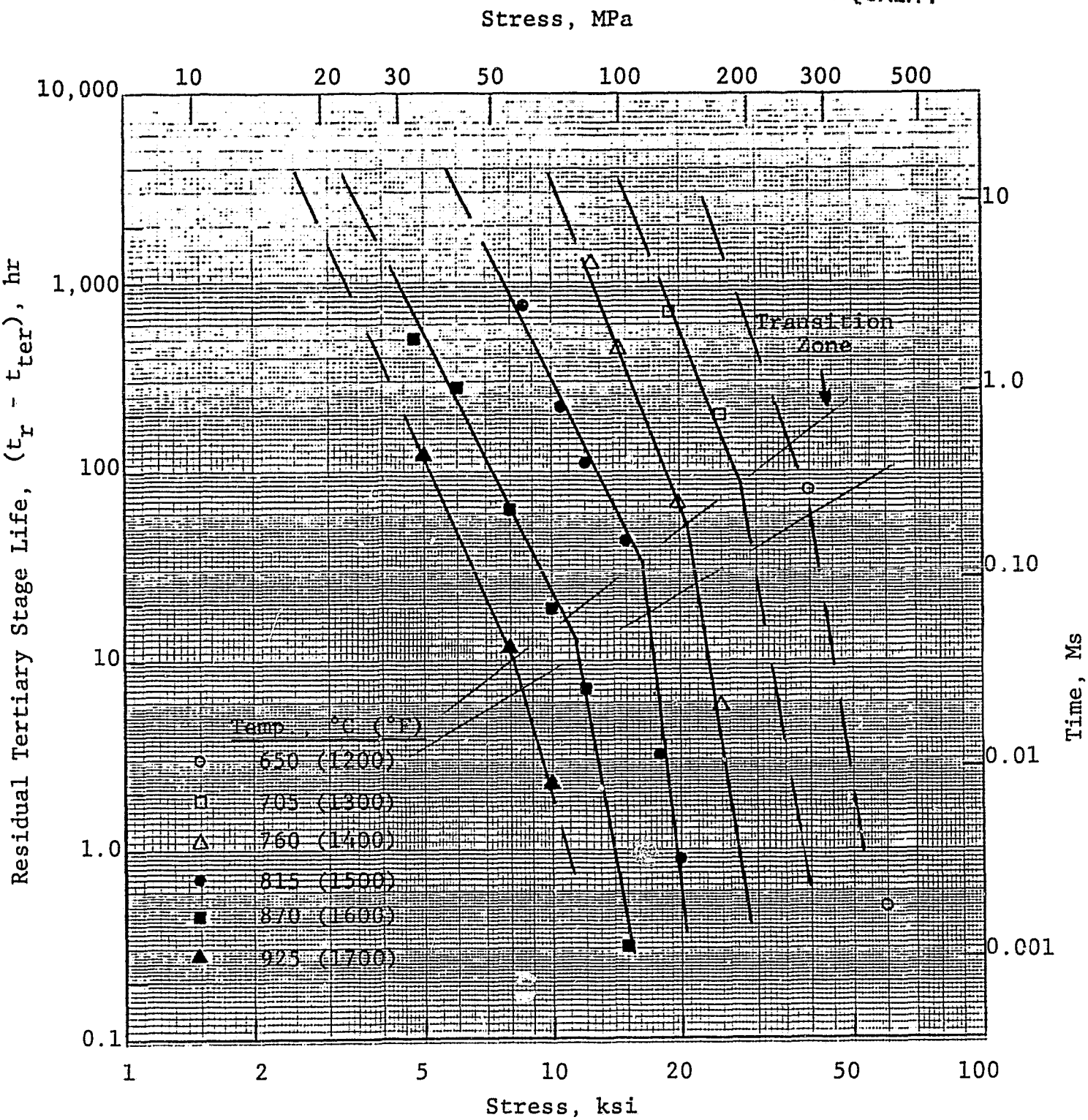

Figure 10

Stress vs. Residual Tertiary Stage Life $(t_r - t_{ter})$, 19-9DL, Unaged (G.S. 33 μm)

an estimated fit to the data point and when all the data become available, statistically fitted lines will be drawn. However, it appeared that single lines at each temperature might not give the best fit and two lines with different slopes were drawn. In other words, at certain stress levels (which is a function of temperature) the stress exponent changes in magnitude. Above the transition zone, an increase in stress decreases residual life at a slower rate than an equivalent stress increase below the transition zone. With more data, a more precise location of the transition zone can be obtained and its meaning in terms of tertiary residual life established.

Total elongation after rupture is plotted vs. stress for each temperature in Fig. 11. Estimated lines were fitted to the data. The data show considerably more scatter than rupture life. Specimen elongation is a more sensitive property than rupture life, and the scatter represents that phenomenon. All these data were for single tests. Duplicate tests will significantly increase confidence levels, and a few replicate tests at two selected temperatures will not only be helpful but also desirable.

Minimum creep rate ($\dot{\varepsilon}_m$) data for each temperature were plotted vs. stress in Fig. 12. Statistically fitted lines were drawn with R^2 values between 0.97 and >0.99. The slope at 815°C (n = 8.85) is higher than the slopes at other temperatures, and the reason for this variation is not clear. At high stresses and temperatures, the time range for secondary creep stage decreases very fast (see Fig. 6), and the high minimum creep rates obtained under such conditions had some degree of uncertainty associated with them.

A creep elongation of 5% in 3500 hr, wholly under a secondary creep condition, is equivalent to 4 E-09 s^{-1}. Figure 12 projects the following stress levels for the different temperatures which will cause such a creep rate: 705°C-145 MPa (21 ksi), 760°C-79 MPa (11.5 ksi), 815°C-47 MPa (8.2 ksi),

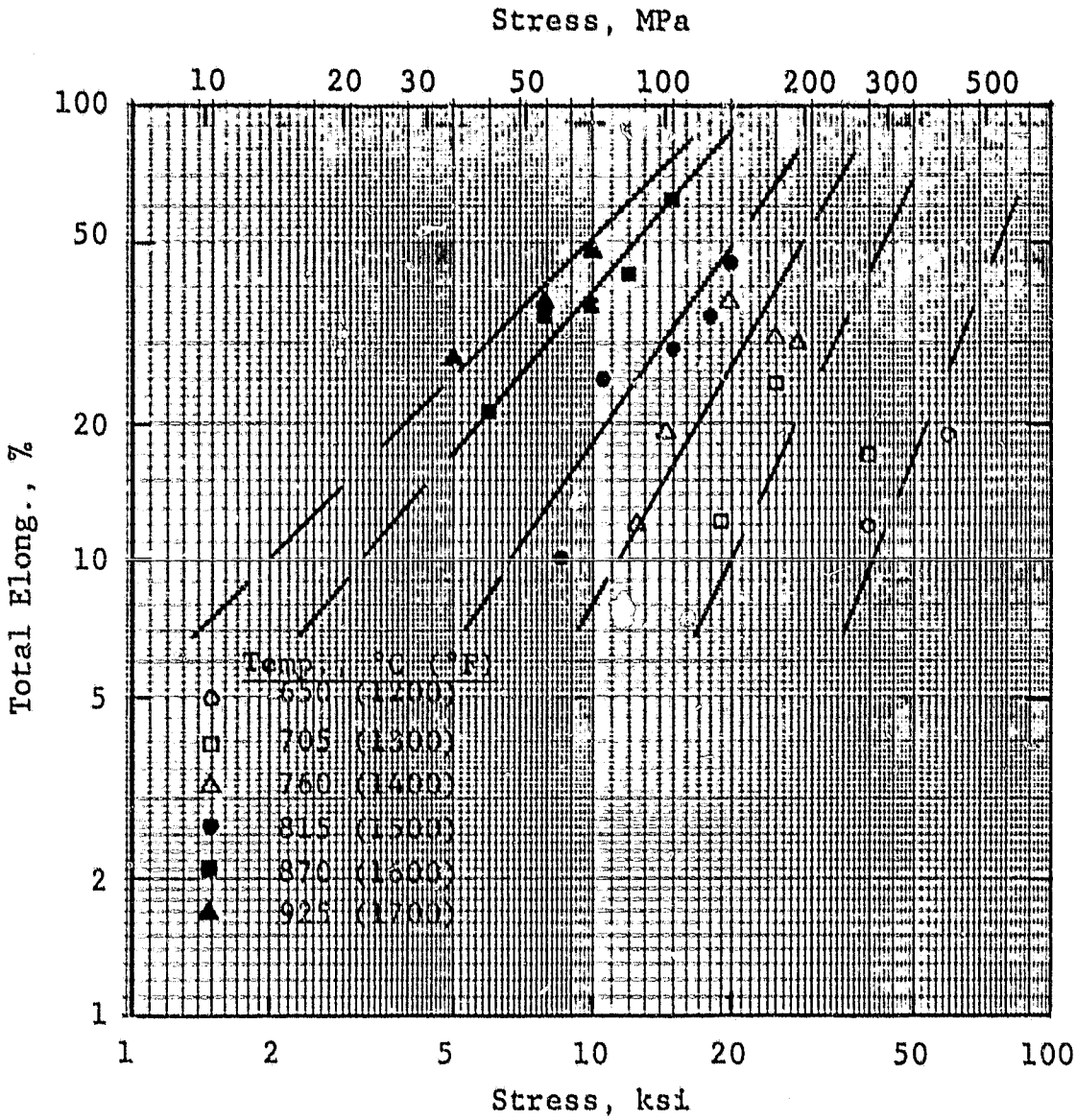

Figure 11

Stress vs. Total Elongation, 19-9DL, Unaged (G.S. 33 μm)

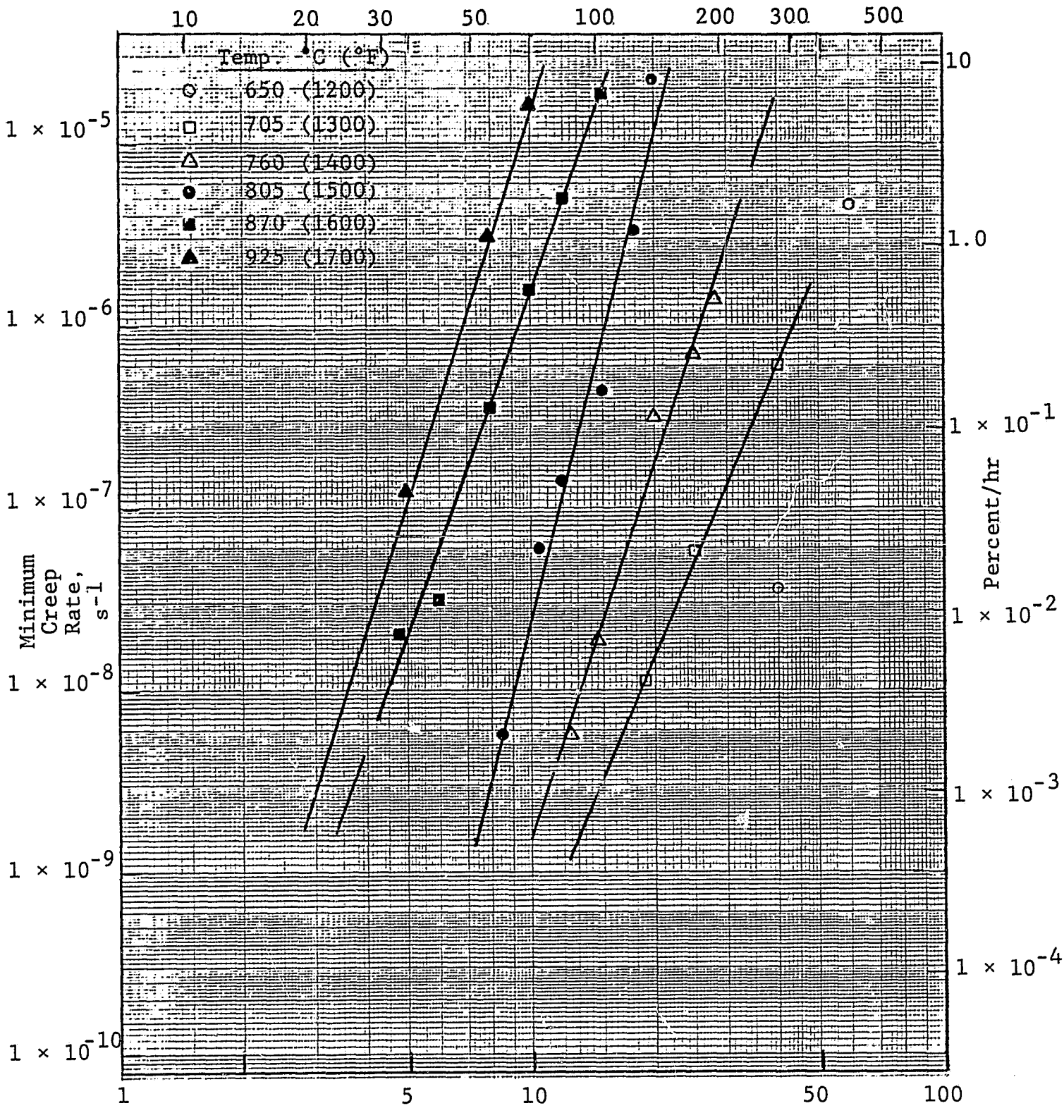

Figure 12

Stress vs. Minimum Creep Rate, 19-9DL, Unaged (G.S. 33 μm)

870°C-27 MPa (3.9 ksi), and 925°C-22 MPa (3.2 ksi). If one considers MOD 1 Stirling engine operation parameters of a 58.5 MPa[1] stress for 4000 hr rupture life at 770°C, then 19-9DL alloy will give the requisite 3500 hr operation life with no greater than 5% elongation at temperatures of about 800°C and below. The very significant difference between the 815° and 870°C $\dot{\varepsilon}_m$ vs. σ relationship requires more testing at these two temperatures.

In the earlier analyses, stress was correlated with various observed parameters such as t_r, $t_{0.01}$, t_{ter}, $t_r - t_{ter}$, ε_t, and $\dot{\varepsilon}_m$. However, these parameters are also interrelated and knowledge of these relationships is of importance to a proper understanding of the creep process.

In Fig. 13, $t_{0.01}$ was correlated with t_r. A single line appeared to fit the data point with $R^2 = 0.89$. The relationship is given by the follcwing equation:

$$t_{0.01} = 0.02\ t_r^{1.26} \qquad (2)$$

Equation 2 implies that a tenfold increase in rupture life will increase $t_{0.01}$ 18-fold. Thus, if a certain minimum $t_{0.01}$ had to be met, the stress/temperature levels could be selected to obtain the desired rupture life.

Parameter $t_{0.01}$ is also correlated with $\dot{\varepsilon}_m$, the minimum creep rate, in Fig. 14. Also, in this plot, a single relationship with an excellent $R^2 = 0.99$ is obtained with one data point excluded from the analysis. The fitted equation is:

$$t_{0.01} = 3.21\ \text{E-06}\ \dot{\varepsilon}_m^{-0.97} \qquad (3)$$

If the exponent -0.97 in Equation 3 is approximated to -1, then Equation 3 can be rearranged thus:

$$t_{0.01} \times \dot{\varepsilon}_m = \text{constant} \qquad (4)$$

and the dimensionless constant for 19-9DL is 3.21 E-06, where

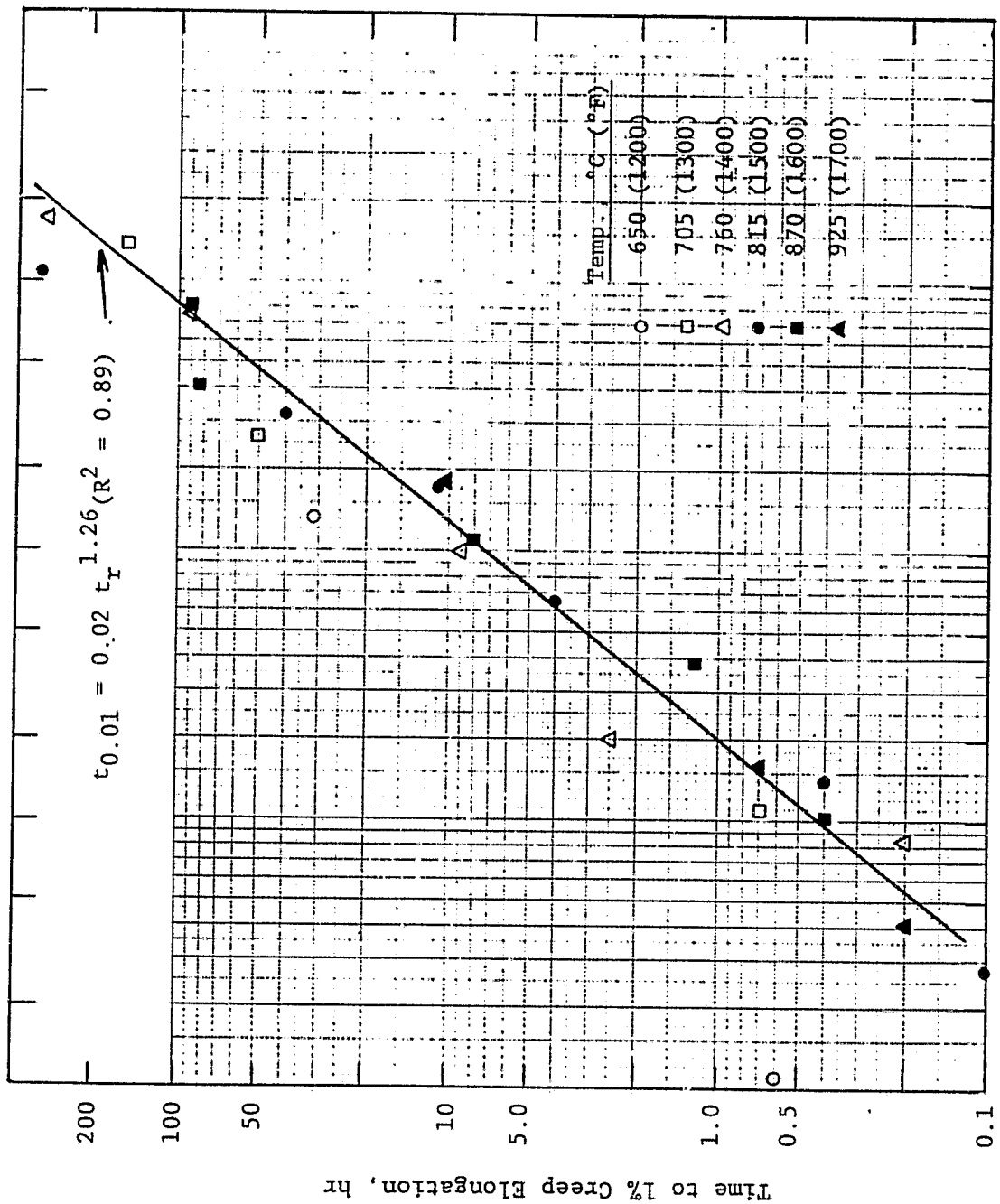

Figure 13

Rupture Life vs. Time to 1% Creep Elongation, 19-9 DL, Unaged (G.S. 33 μm)

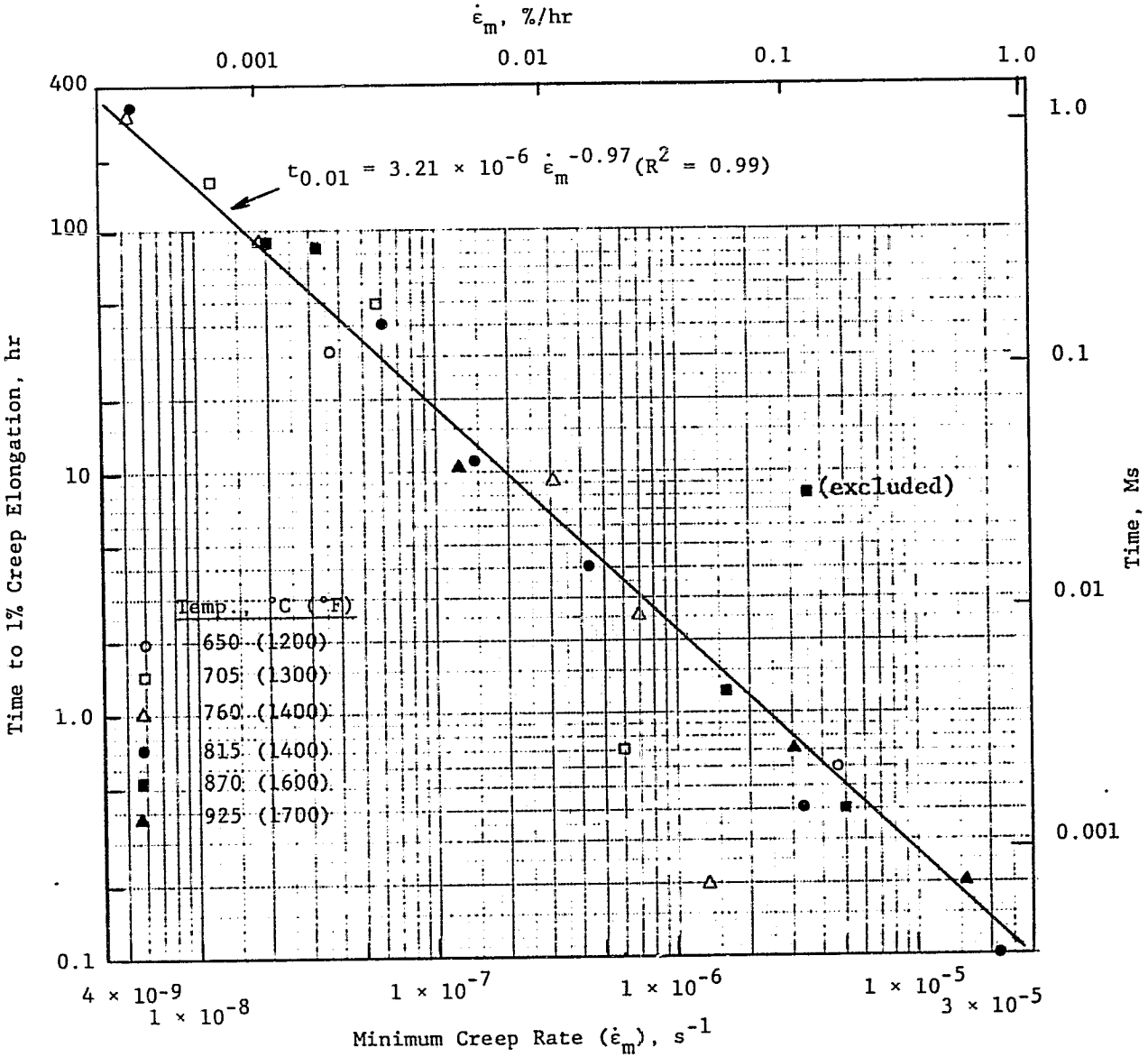

Figure 14

Minimum Creep Rate vs. Time to 1% Creep Elongation, 19-9 DL, Unaged (G S. 33 μm)

$t_{0.01}$ is in hr and $\dot{\varepsilon}_m$ is expressed in s^{-1}. If, however, $t_{0.01}$ is expressed in seconds, then the constant will be 1.16 E-02.

A rearrangement of Equations 2 and 3 can also be made to obtain the following:

$$\dot{\varepsilon}_m \times t_r^{1.26} = \text{constant} \qquad (5)$$

under the assumption that the exponent -0.97 is considered equal to -1.0. Thus, a knowledge of either $\dot{\varepsilon}_m$ or t_r permits one to obtain the other. However, more data are needed for this analysis.

Finally, Fig. 15 shows the correlation between the residual tertiary stage life $(t_r - t_{ter})$ and the total elongation, ε_t. All the different temperatures (with the exclusion of two 650°C data) appeared to fit a single line which had two different slopes. Approximately at 100 hr, there appeared to be a change in the slope. For shorter $(t_r - t_{ter})$ lives, the rate of increase in total elongation with life is less. For example, between 1000 and 100 hr, the total elongation increased from 10 to 30%. But between 100 and 10 hr, ε_t increased from 30 to 38%. Most of the high elongation data belonged to the high temperature tests. This change in slope for the low temperature data may be associated with a change in the deformation mechanism. In a recent analysis, Pizzo[2] had analyzed 304 SS data using nine different models and none of them were found to be satisfactory. A fitted model was found to be the best. A very much larger data base than that presently available will be needed for this form of analysis for 19-9DL.

[2] P. P. Pizzo, "Rate Equations for Elevated Temperature Creep," Trans. ASME, Vol. 101, No. 4, Oct. 1979, pp. 396-402.

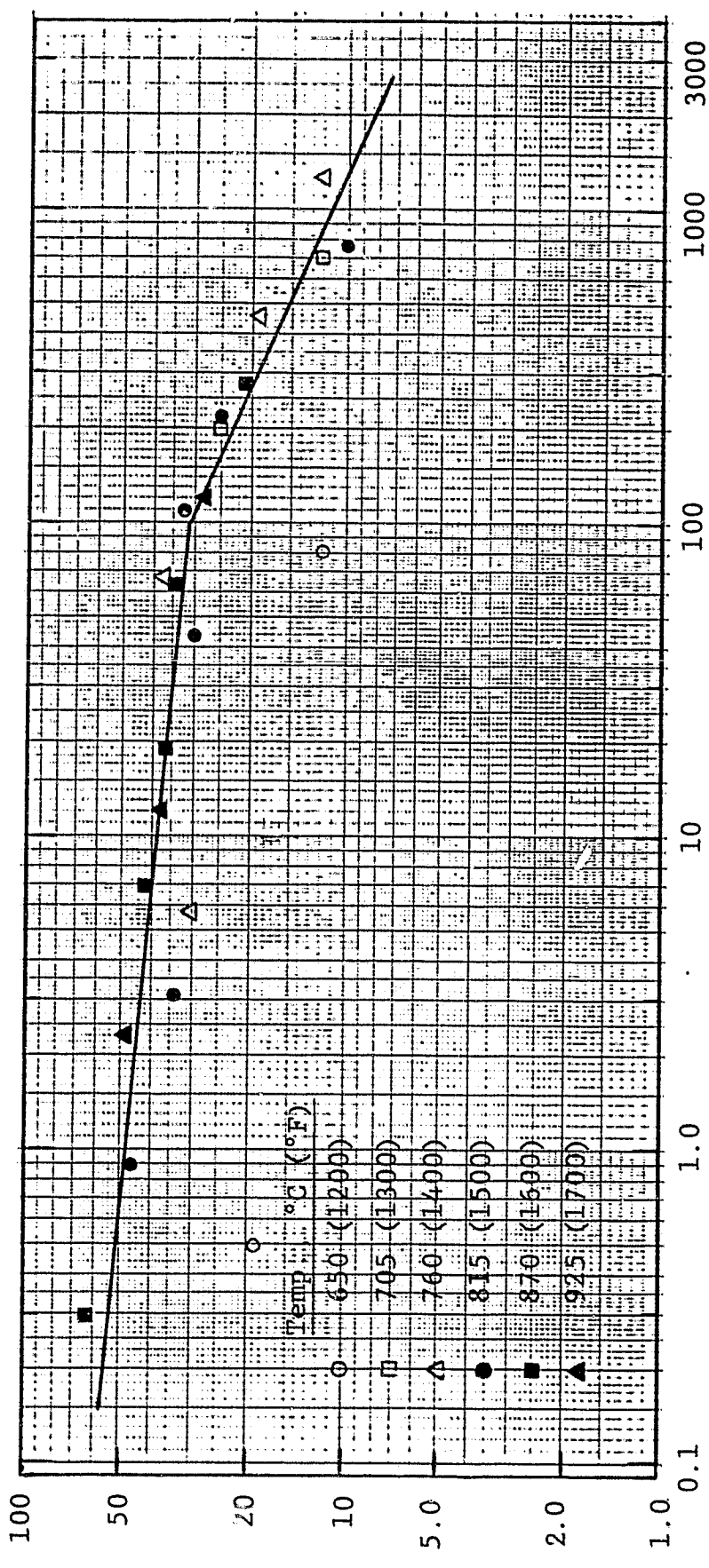

Figure 15

Total Elongation as a Function of Residual Tertiary Stage Life, 19-9DL, Unaged (G.S. 33 μm)

2.3.2 Statistical Analysis of Temperature-Compensated Rupture Life Data

Temperature-compensated rupture life analysis in its simple form utilizes a relationship

$$t = \text{constant} \cdot (\text{stress})^n \cdot e^{Q/RT} \qquad (6)$$

where n is the stress exponent, Q is the activation energy controlling the process, and t is time to rupture or to a specific creep elongation. Details of this relationship are given in Appendix B.

All twenty-five 19-DL t_r data and the twenty-four $t_{0.01}$ data were analyzed according to Equation 6, and the results are summarized in Table 5. The data were also analyzed with different restrictions on stress levels, rupture life, or both.

Table 5 shows that the best R^2 of 0.96 was obtained for t_r when data for stress levels of 276 MPa and above were excluded. Restriction of data to $t_r \geq 10$ hr improved R^2 to 0.91 from 0.87 of total data analysis. Combined restrictions of both stress and rupture life shown under item 4 of Table 5 did not improve correlation over the item 2 value with stress restriction only.

Under the best correlation, stress exponent n_2 was -5.70 for t_r and -7.15 for $t_{0.01}$. The activation energy associated with t_r was 438 kJ/°K-mole and for $t_{0.01}$, a higher value of 558 kJ/°K-mole.

As shown in Appendix B, the rearrangement of Equation 6 will results in the following:

$$\ln \sigma = \frac{1}{n_2} \left(\ln t_r - \frac{Q_2}{RT}\right) - \text{constant} \qquad (7)$$

and when $(\ln t_r - Q_2/RT)$, the temperature-compensated rupture life is plotted against $\ln \sigma$, a linear relationship is obtained, as shown in Fig. 16.

In Fig. 16, the 22 data (item 2, Table 5) were plotted and the slope of the line is n_2, the stress exponent. The R^2 value for the fitted line is 0.98. This value may be considered very good for the wide stress range of 35 to 276 MPa and temperature

Table 5

ALLOY 19-9DL: TEMPERATURE-COMPENSATED STATISTICAL ANALYSIS OF RUPTURE LIFE AND TIME TO REACH 1% CREEP ELONGATION

Analytical Mode	Term[a]	Data Base	Constant ($\ln k_2$)	Stress Exponent (n_2)	Activation Energy (Q_2), kJ/°K-mole	Corr. Coeff. (R^2)
1. No Restriction	t_r	25	-13.1	-6.16	406	0.87
	$t_{0.01}$	24	-24.5	-7.45	538	0.92
2. Stress below 276 MPa (40 ksi)	t_r	22	-18.6	-5.70	438	0.96
	$t_{0.01}$	21	-27.9	-7.15	558	0.94
3. Rupture life ≥3.6 E-02 Ms (10 hr)	t_r	20	-14.1	-5.37	385	0.91
	$t_{0.01}$	20	-25.4	-6.91	525	0.92
4. Stress below 276 MPa and/or rupture life ≥3.6 E-02 Ms	t_r	18	-17.1	-5.12	403	0.95
	$t_{0.01}$	18	-28.1	-6.61	540	0.94

$$\ln t = n_2 \ln \sigma + \frac{Q_2}{RT} + \ln k_2$$

where $t = t_r$ or $t_{0.01}$, σ = stress, n_2 = stress exponent, k_2 = constant, Q_2 = activation energy, T = test temperature, and R = universal gas constant.

[a] t_r = rupture life, $t_{0.01}$ = time to reach 1% creep elongation.

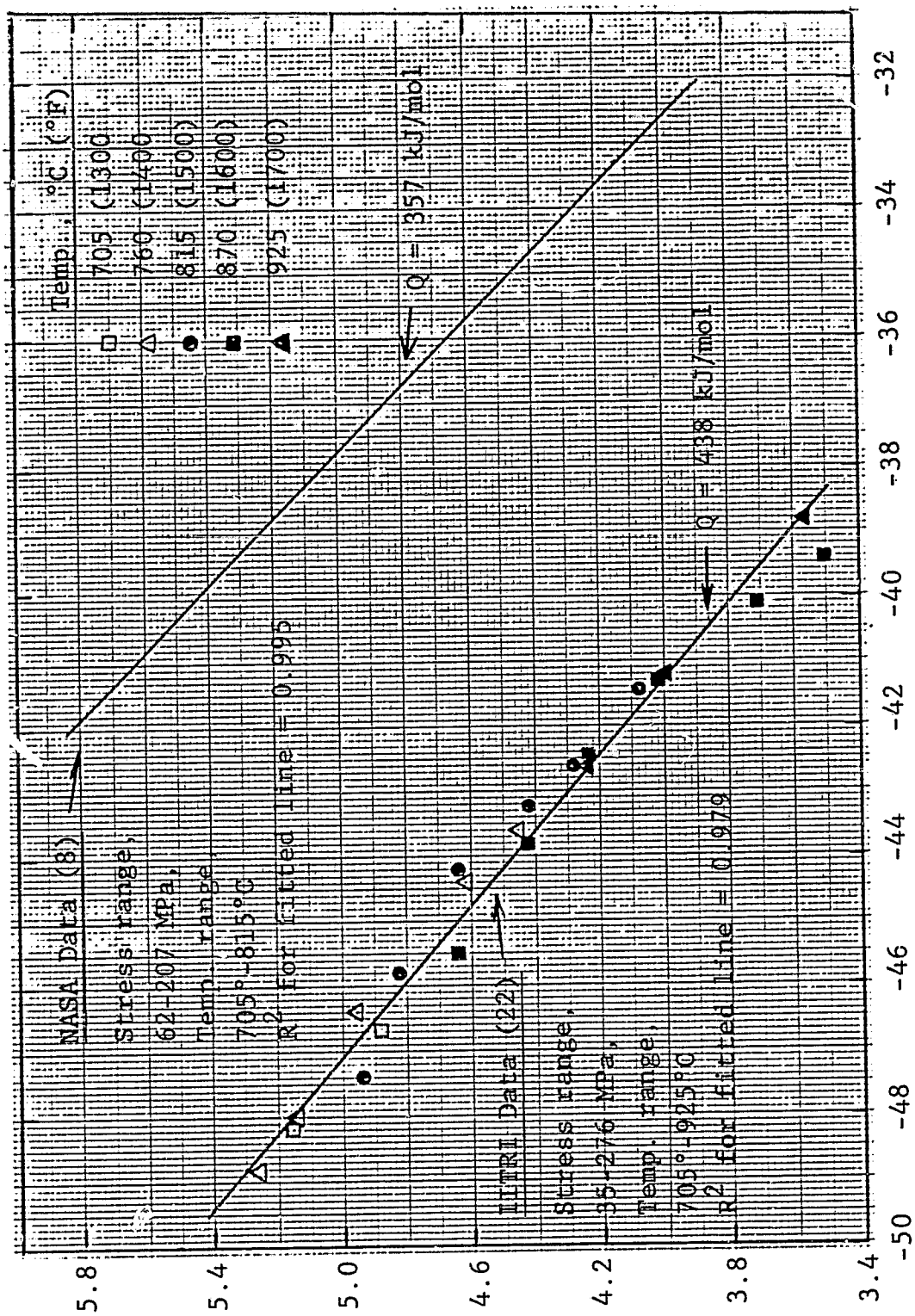

Figure 16

Temperature-Compensated Rupture Life vs. Stress, 19-8DL, Unaged, (G.S. 33 μm)

range of 705°-925°C. For comparison, NASA data were also plotted showing that the stress exponent n_2 is very similar to that of IITRI data. The lower Q_2 value of NASA data had shifted the line to the right but kept it parallel to the IITRI data. The essential similarity between IITRI and NASA data is very significant.

A similar analysis (see Appendix B) of $\dot{\varepsilon}_m$ data was conducted and the results are given in Table 6. Figure 12 showed earlier that $\dot{\varepsilon}_m$ vs. σ at each temperature had more variability, the temperature-compensated analysis R^2 values were lower than that for rupture life data. Elimination of stress levels above 276 MPa improved R^2 from 0.76 to 0.80, but still it was below the observed R^2 = 0.95 of NASA data. However, the Q_2 value of -408 kJ/°K-molewas close to the NASA value of -417 kJ/°K-mole.

2.3.3 Statistical Analysis of Rupture Life Data for Alloys A-286, IN 800H, N-155, CRM-6D, and XF-818

Rupture life data from Appendix A were plotted in Figs. 17 to 21 for five different alloys. Regression lines were fitted to the data points.

In Fig. 17, four lines were fitted to the A-286 data at 705° to 870°C. Sufficient data were not yet available to fit the 650° and 925°C temperatures. The R^2 values for the fitted lines were between 0.93 and 0.99. It may be seen that several tests in A-286 were terminated earlier, and these data were not used in fitting the lines. However, information contained in these tests in the form of time to various creep elongation levels, minimum creep rates, and other parameters were available and will be used in the final analysis. The stress exponents varied between -4.46 (815°C) and -7.65 (705°C). All the stress exponents at each temperature are summarized in Table 7.

The IN 800H data are shown in Fig. 18. The R^2 values for the six fitted lines ranged from 0.93 to 0.99. The significant change in slope at the higher temperature is reflected in the stress-life exponent values given in Table 7.

Table 6

ALLOY 19-9DL: TEMPERATURE-COMPENSATED ANALYSIS OF MINIMUM CREEP RATE DATA

	Analytical Mode	Data Base	Constant ($\ln k_2$)	Stress Exponent (n_2)	Activation Energy (Q_2), kJ/°K-mole	Corr. Coeff. (R^2)
1.	No restriction	25	8.70	5.90	-452	0.76
2.	Stress below 276 MPa (40 ksi)	22	12.7	5.60	-477	0.80
3.	Rupture life ≥3.6 E-02 Ms (10 hr)	20	7.98	4.90	-408	0.71
4.	Stress below 276 MPa and/or rupture life ≥3.6 E-02 Ms	18	9.58	4.79	-418	0.71
5.	NASA 19-9DL (Ht-2), 62-207 MPa range	8	4.40	5.90	-417	0.95

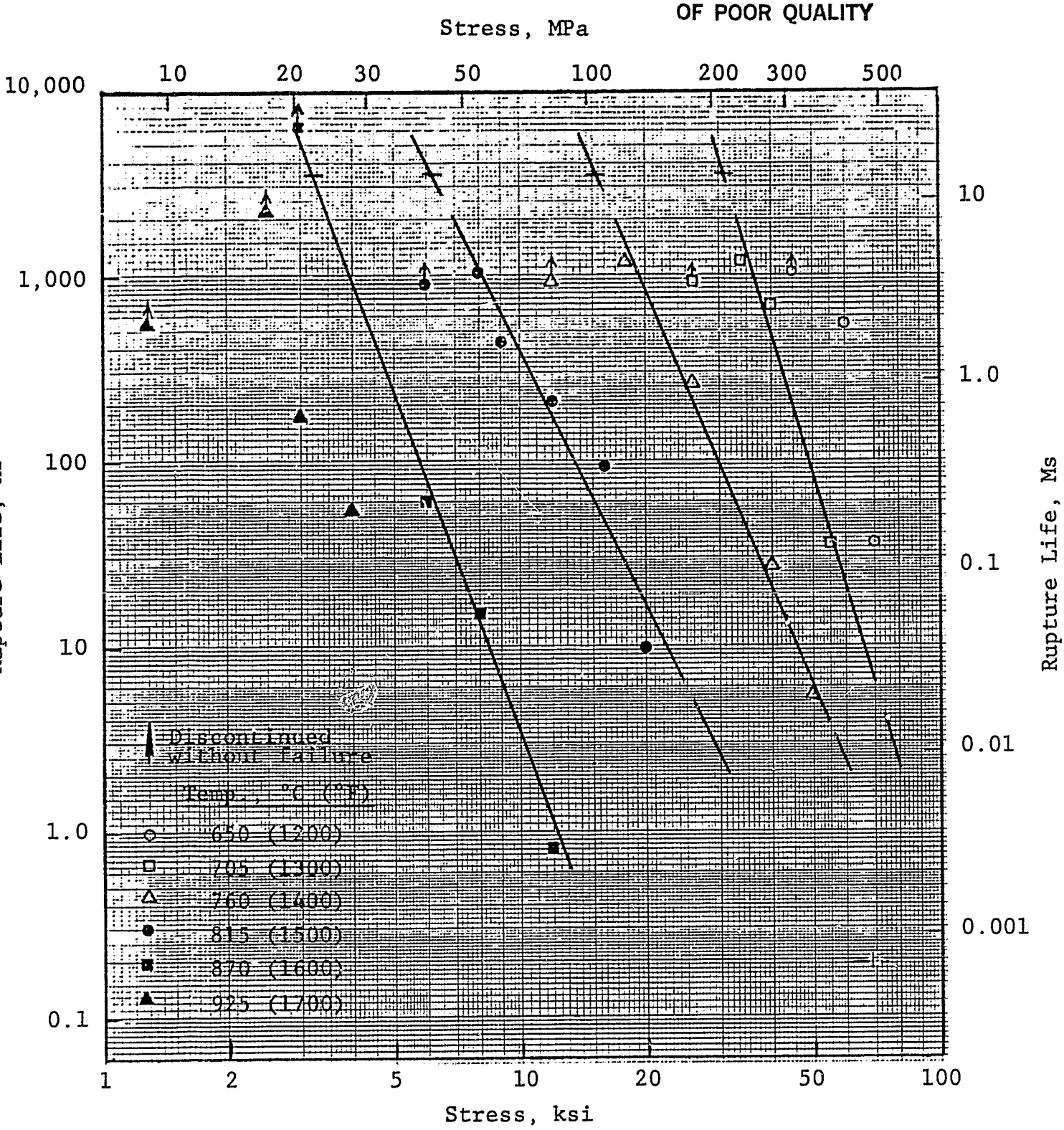

Figure 17

Stress vs. Rupture Life, A-286, Unaged (G.S. 72 μm)

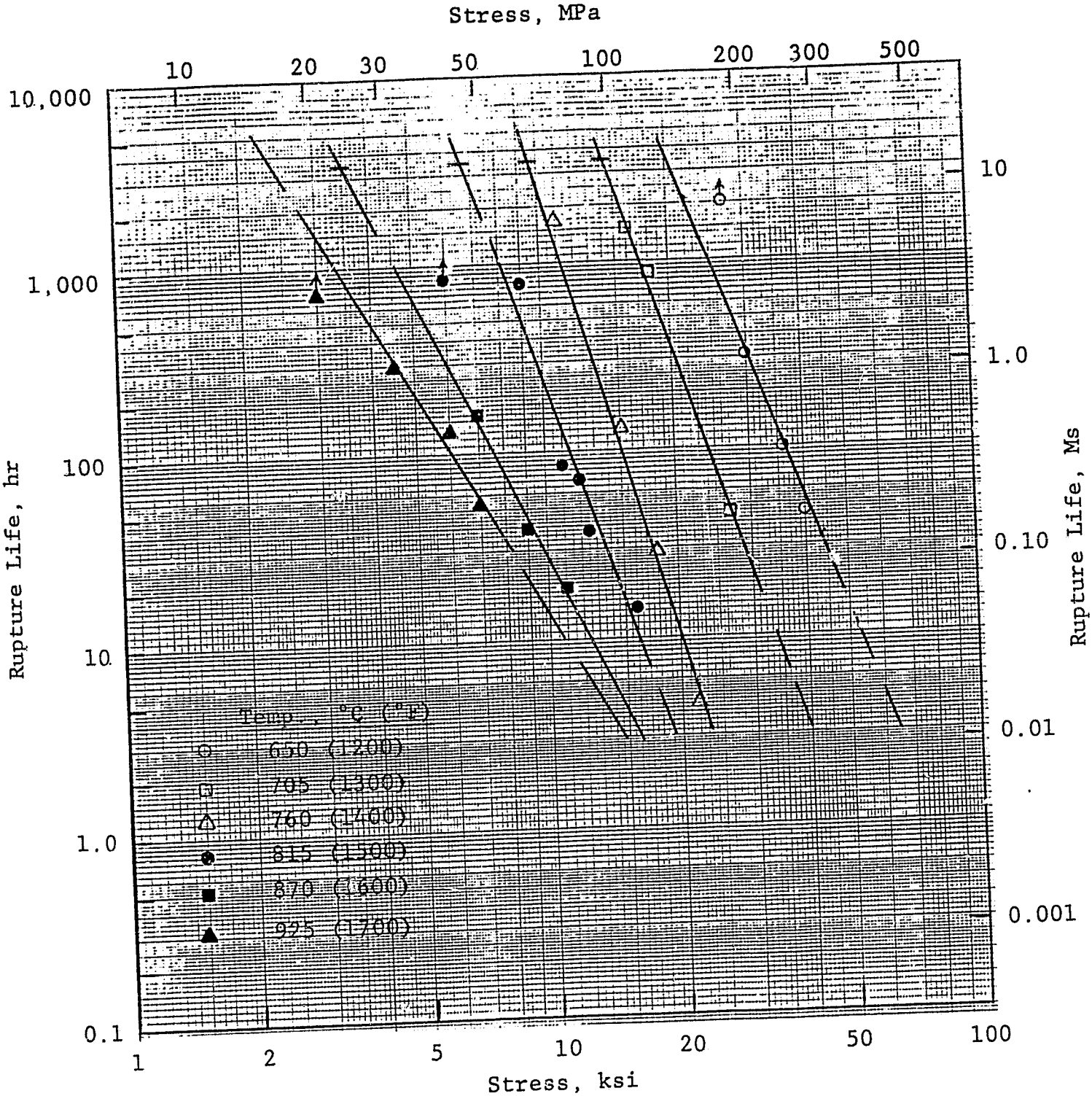

Figure 18

Stress vs. Rupture Life, IN 800H, Unaged (G.S. 64 μm)

Table 7

STRESS EXPONENTS AT DIFFERENT TEMPERATURES
FOR THE SIX ALLOYS

Alloy	Stress Exponent at Given Temperatures[a]					
	650°C (1.083)	705°C (1.022)	760°C (0.968)	815°C (0.919)	870°C (0.875)	925°C (0.835)
A-286	ND	-7.65	-5.20	-4.46	-6.18	ND
IN 800H	-6.03	-6.74	-8.04	-6.82	-4.65	-3.79
N-155	-14.2	ND	-6.29	-6.02	-6.45	-4.73
19-9DL	ND	-6.49	-6.55	-6.53	-5.26	-5.51
CRM-6D	ND	-12.7	-12.5	-10.3	-10.1	ND
XF-818	ND	-15.3	-8.48	-7.01	-6.25	ND

ND - no data.

[a]Figures in parentheses are reciprocals of temperature: $1000/T$, $°K^{-1}$, where T is in °K.

The N-155 data are shown in Fig. 19. The NASA data are also shown in Fig. 19 and indicate the good agreement between the IITRI and NASA data. The R^2 values for IITRI lines were between 0.98 to >0.99. The stress exponents had varied, and these data are given in Table 7.

The limited CRM-6D data are shown in Fig. 20. The four fitted lines had very high R^2 values of 0.99 and higher. More data will be needed to correlate 925° and 650°C rupture lives. The stress-life exponents were much higher than the wrought alloys and are summarized in Table 7.

The four fitted lines for XF-818 are shown in Fig. 21. The R^2 values ranged from 0.97 to >0.99. The stress exponent increased with increasing temperature and was higher than CRM-6D; the values are summarized in Table 7.

All the rupture life-stress exponents for each alloy and temperature given in Table 7 are plotted in Fig. 22 as a function of 1/T. There is significant scatter in the data with CRM-6D forming a separate set. For temperatures in the range of 760° to 925°C, a broad trend may be seen. A statistically fitted line could be drawn when more data become available. An estimated envelope drawn over the data indicated an activation energy of about 40-50 kJ/°K-mole. Thus, the activation energy, or in other words, the effect of temperature on stress-life exponent, was much smaller than the effect of temperature on rupture life where the activation energy was observed to be about 10 times larger, i.e., about 400-500 kJ/°K-mole.

2.3.4 Statistical Analysis of Temperature-Compensated Rupture Life Data for Alloys N-155 and XF-818

Similar to the analysis for 19-9DL, the data for N-155 and XF-818 were analyzed according to the equation given in Appendix C.

The N-155 analysis is summarized in Table 8 and XF-818 in Table 9. In Table 8, an analysis of NASA data is also included to compare the grain size effect.

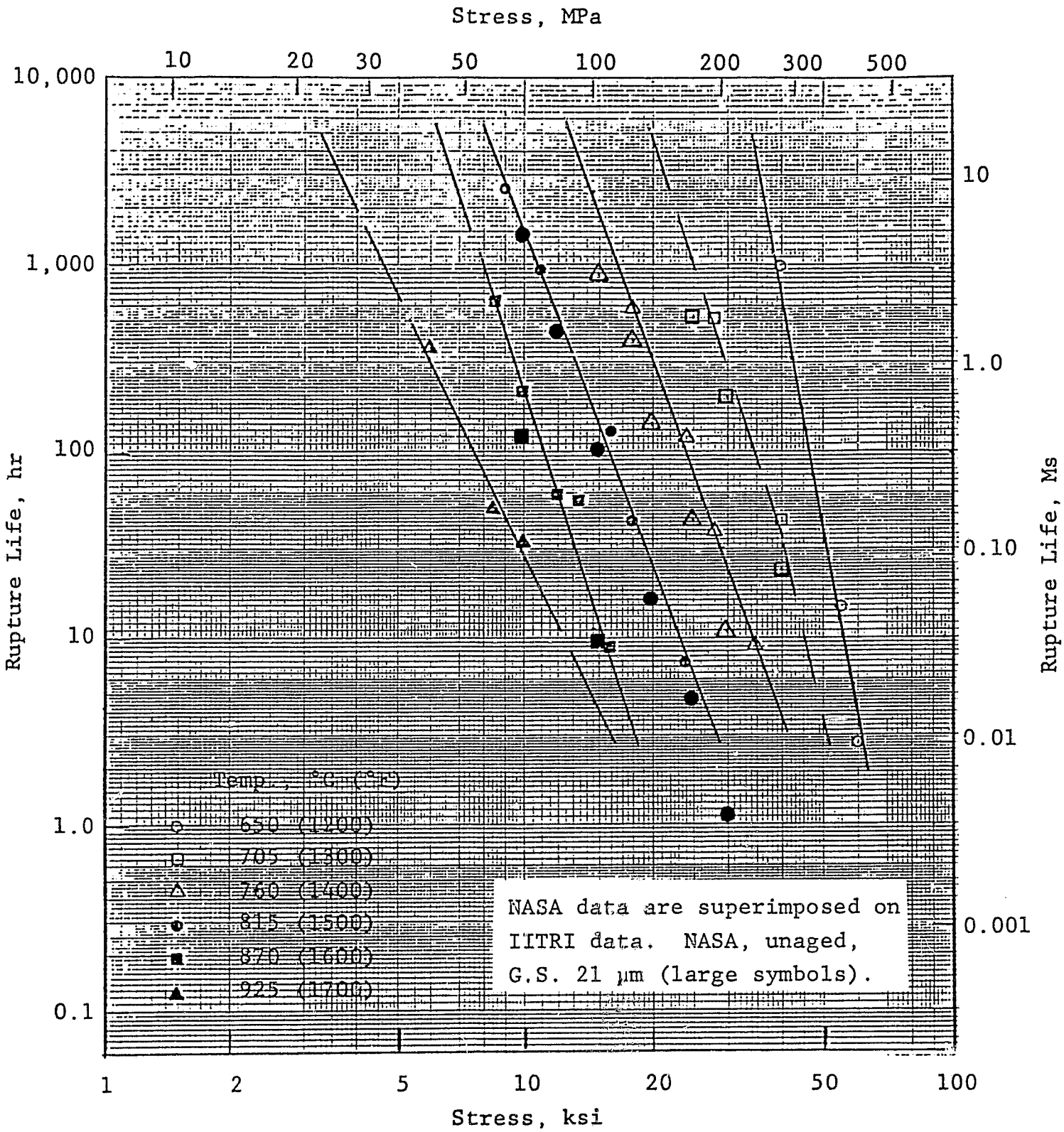

Figure 19

Stress vs. Rupture Life, N-155, Unaged (G.S. 42 μm)--
A Comparison of IITRI and NASA Data

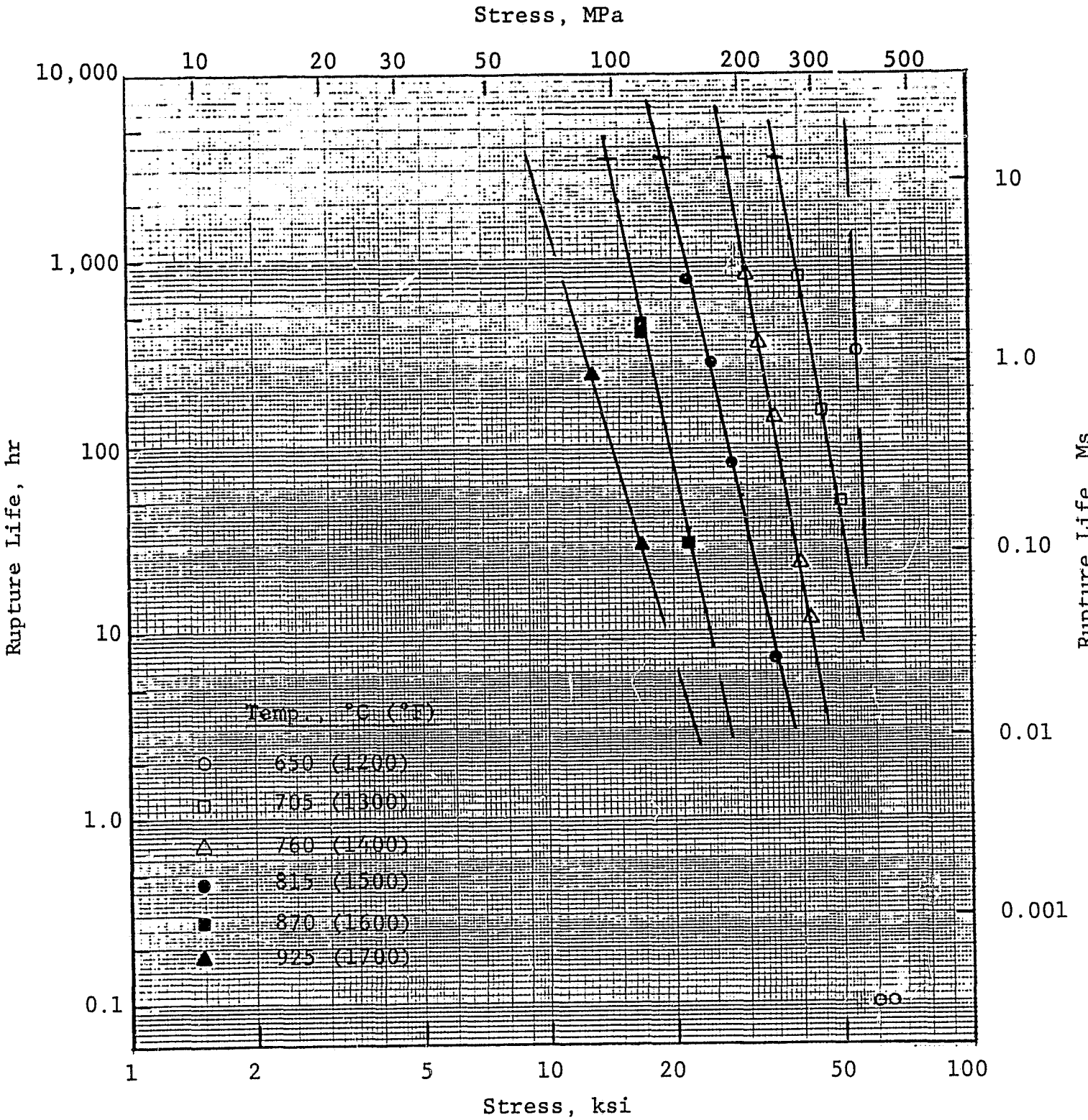

Figure 20

Stress vs. Rupture Life, CRM-6D, Aged,
650°C (1200°F), 0.36 Ms (100 hr)

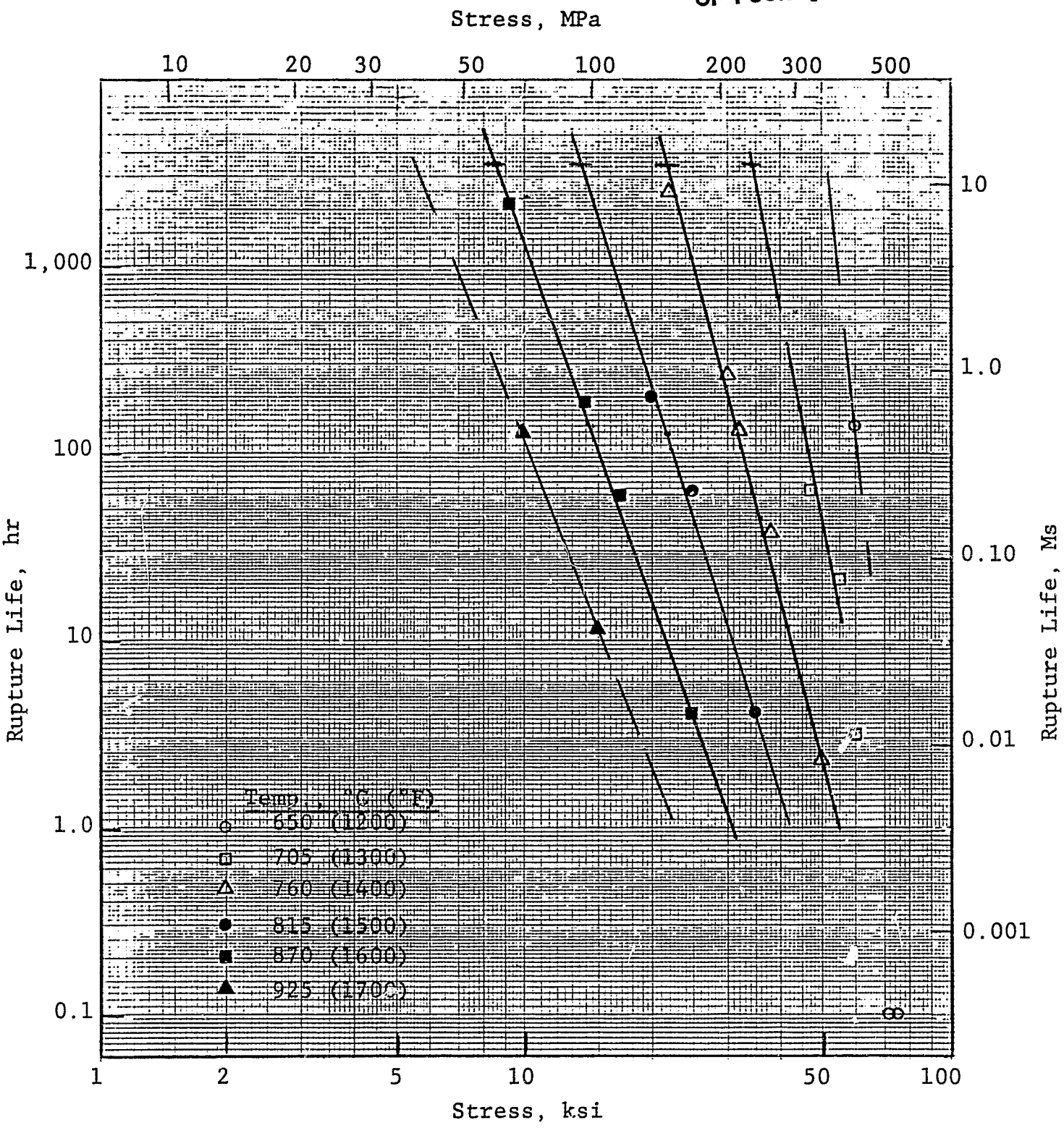

Figure 21

Stress vs. Rupture Life of XF-818, As Cast

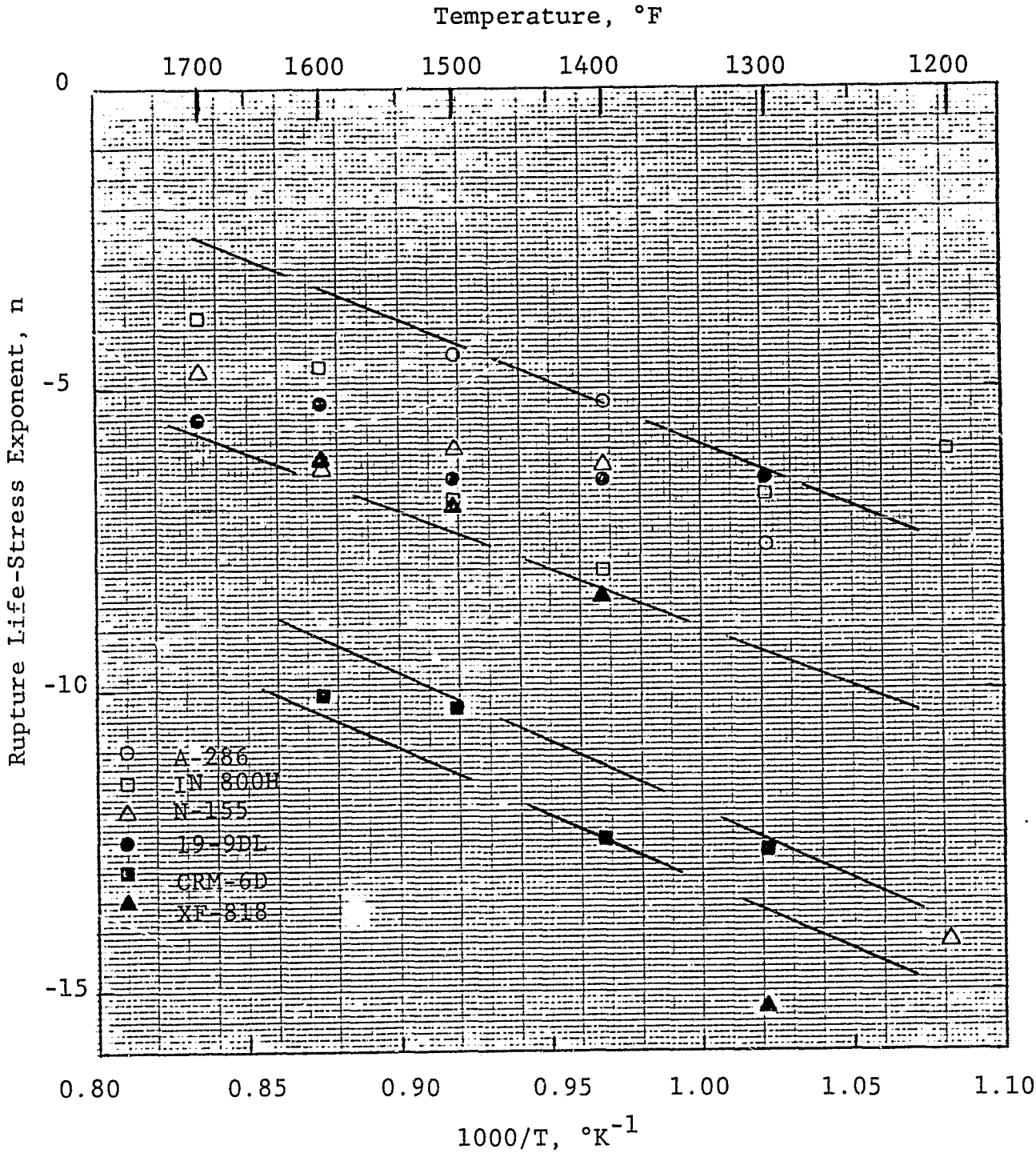

Figure 22

Effect of Temperature on Rupture Life-Stress Exponent in Six Different Alloys

Table 8

ALLOY N-155: TEMPERATURE-COMPENSATED STATISTICAL ANALYSIS OF RUPTURE LIFE

	Analytical Mode	Data Base	Constant ($\ln k_2$)	Stress Exponent (n_2)	Activation Energy (Q_2), kJ/°K-mole	Corr. Coeff. (R^2)
1.	All data	23	-6.55	-6.28	366	0.83
2.	Stress below 345 MPa (50 ksi)	21	-11.6	-5.95	399	0.98
3.	Rupture life ≥3.6 E-02 Ms (10 hr)	19	-8.6	-6.02	375	0.86
4.	Stress below 345 MPa and/or rupture life ≥3.6 E-02 Ms	18	-11.0	-5.71	384	0.97
5.	NASA (G.S. 21 μm) Stress range 69-276 MPa	16	-10.1	-6.40	400	>0.99

Table 9

ALLOY XF-818: TEMPERATURE-COMPENSATED STATISTICAL ANALYSIS OF RUPTURE LIFE

Analytical Mode	Data Base	Constant ($\ln k_2$)	Stress Exponent (n_2)	Activation Energy (Q_2), kJ/°K-mole	Corr. Coeff. (R^2)
1. All data less 2 tests which failed on loading	18	-6.98	-7.01	422	0.90
2. Stress below 414 MPa (60 ksi)	16	-11.4	-7.04	463	0.96
3. Rupture life ≥3.6 E-02 Ms (10 hr)	14	-7.56	-6.38	399	0.86
4. Stress below 414 MPa and/or rupture life ≥3.6 E-02 Ms	13	-11.6	-6.86	460	0.93

Data in Table 8 show that when the stress level of N-155 was restricted below 355 MPa, the R^2 value increased from 0.83 for all 23 data to 0.98 for 21 data. Hardly any improvement was observed when rupture life restriction was included.

A comparison with NASA data shows that the smaller grain size resulted in a somewhat lower rupture life. The activation energy was not affected by the grain size change though the stress-life exponent slightly decreased. Combined NASA and IITRI data (37 tests) resulted in Q = 402 kJ/°K-mole, n = -6.02, and R^2 = 0.97.

The XF-818 data analysis showed that when the stress level was restricted below 414 MPa, the R^2 value improved from 0.90 to 0.96. Restriction on rupture life instead of improving correlation actually resulted in a decrease in R^2 value. Additional data will improve the overall correlation.

2.3.5 Predicted Rupture Stress for 3500 hr Rupture Life in Different Alloys

The stress-life data shown in Figs. 7, and 17 to 21 were extrapolated at four different temperatures to obtain the stress levels for 3500 hr rupture lives. These values are summarized in Table 10.

The results show that at 760°C, all the alloys have rupture stresses higher than 60 MPa. It has been mentioned earlier[1] that the MOD 1 Stirling engine is designed for 770°C/4000 hr/58.5 MPa operation, and the six alloys all appear to be very close to this value. However, at a higher temperature of 815°C, only three alloys meet the 58.5 MPa requirement and these are N-155, XF-818, and CRM-6D. Alloy 19-9DL had a predicted rupture stress of 52 MPa which could possibly be adequate. At the high temperature of 815°C, only the two cast alloys retained significant strength, while A-286, IN 800H, and 19-9DL decreased in strength very significantly, and N-155 somewhat more slowly.

Table 10

PREDICTED RUPTURE STRESS FOR 3500-HOUR RUPTURE LIFE IN THE SIX ALLOYS

Alloy	Stress at Given Temperatures, MPa			
	705°C (1300°F)	760°C (1400°F)	815°C (1500°F)	870°C (1600°F)
A-286	210	110	43	22
IN 800H	100	66	46	24
N-155	140	93	59	46
19-9DL	150	79	52	27
CRM-6D	240	190	130	98
XF-818	230	150	94	59

2.3.6 Fractographic Analysis of Creep-Rupture Specimens

Fracture analysis was performed on a selected number of creep-rupture specimens of various alloys tested in air. The purpose of this examination was to study the modes and mechanisms of failure in each case and their dependence on alloy composition, fabrication (wrought or cast), stress, and test temperatures. Typical fracture failures from alloy 19-9DL and XF-818 are presented and discussed in this section.

Figure 23 presents typical fractographs of the 19-9DL alloy specimen creep rupture tested at 760°C and 86.2 MPa. This specimen failed in 1687 hr and exhibited an elongation of 10.9%. Figure 23a shows the two mating fractured surfaces of the above specimen. Macro examination at lower magnifications showed a rough and granular fracture which was dark gray. This fracture seemed to have originated at multiple locations near the specimen surface. Small and relatively smoother areas were observed near various origins such as that shown in Fig. 23b, the origin area at the top right-hand corner of Fig. 23a (B). At this point, the fracture appears to have originated at a large inclusion contained inside a pore. Dimple rupture was the dominant fracture mode over the entire fracture surface. In most areas the fractured surfaces had developed significant amounts of oxides subsequent to failure that masked the finer fracture features. Figure 23c shows a typical microfractograph from the center of the specimen surface shown in Fig. 23a (B). Mainly granular oxides and some fine dimples are clearly visible.

Typical fracture features of 19-9DL alloy specimen creep rupture tested at 815°C and 124 MPa are shown in Fig. 24. Figure 24a (A and B) shows low-magnification macrofractographs of the two mating surfaces. This fracture also seemed to have originated at multiple locations (surface cracks) near the outer edges of the specimen cross-section. Rough topography of the

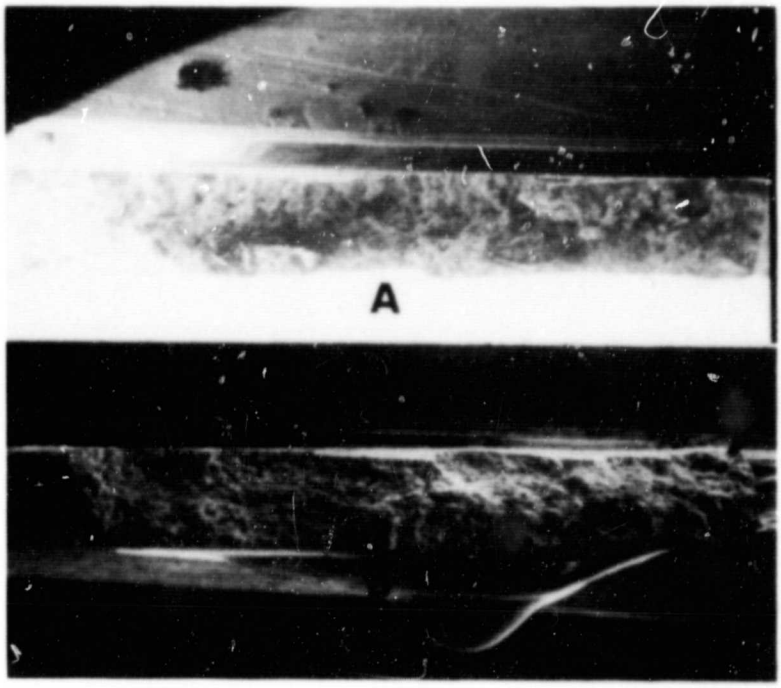

SEM No. 6474, 6475 ~15X

(a)

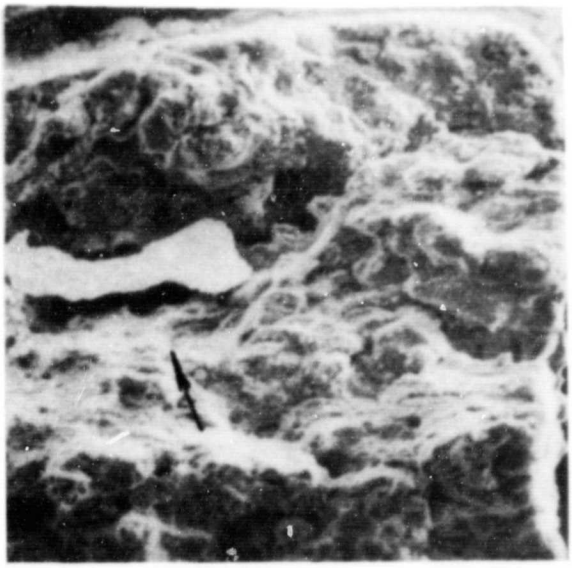

SEM No. 6476 150X

(b)

SEM No. 6478 500X

(c)

Figure 23

Typical Macro- and Microfractographs of the 19-9DL Specimen Creep Rupture Tested at 760°C and 86 MPa. (a) Macrofractographs showing mating fracture surfaces; (b) microfractograph from top right-hand corner of Fig. 23a (B); and (c) microfractograph from the center of Fig. 23a (B).

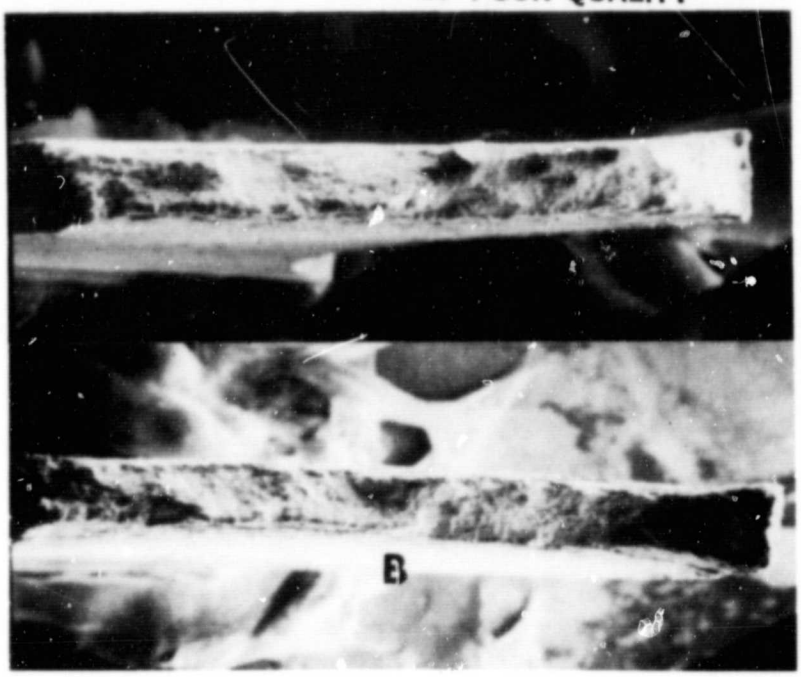

SEM No. 6479, 6480 ~15X

(a)

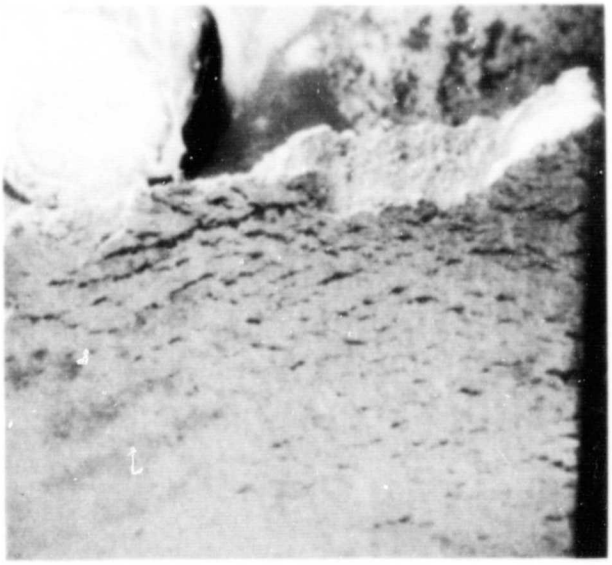

SEM No. 6485 15X

(b)

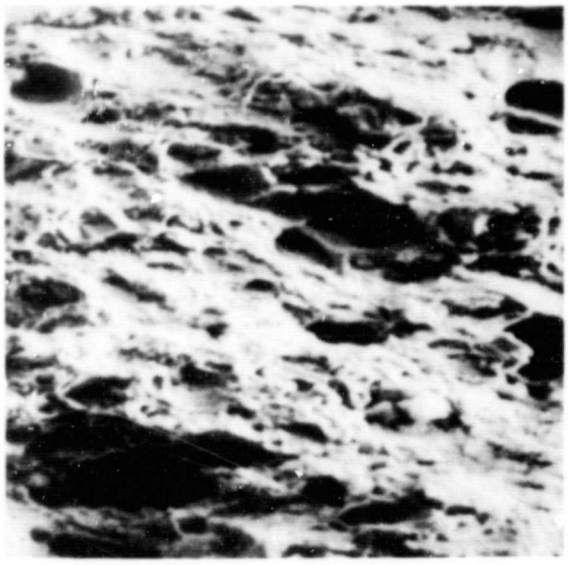

SEM No. 6484 500X

(c)

Figure 24

Typical Macro- and Microfractographs of the 19-9DL Specimen Creep Rupture Tested at 815°C and 124 MPa. (a) Macrofractographs of the mating surfaces; (b) side view of the fracture surface shown in Fig. 24a (B); and microfractographs of areas in Fig. 24a (B); (c) central region of the specimen surface, (d,e) area at upper left corner, and (f) region near right end.

SEM No. 6482 100X

(d)

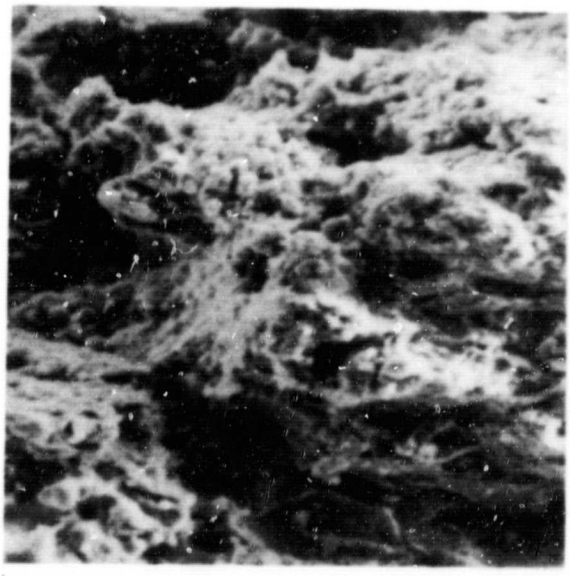

SEM No. 6483 500X

(e)

SEM No. 6481 500X

(f)

Figure 24 (cont.)

fracture and abundance of surface cracks are clearly seen in Fig. 24b, which gives a side view of the fracture shown in Fig. 24a (B). In the central region of the fracture surface (Fig. 24a, B), the fracture occurred primarily by dimple rupture mechanism as illustrated in Fig. 24c. Both clusters of small equiaxed dimples separated by larger elongated dimples containing precipitate particles and inclusions cover the entire area. The area in Fig. 24c also shows some surface oxides that were formed subsequent to fracture. Near the left edge of the specimen (Fig. 24c,B), the fracture appeared very rough and heavily oxidized (Figs. 24d and e), but the main fracture mode was dimple rupture. Formation of heavy surface oxides indicates that the separation of fracture surfaces started in the region shown in Fig. 24d and e. At the right end of the fracture surface in Fig. 24a (B), the main fracture features observed were small elongated dimples with very little surface oxide (Fig. 24f), indicating that the final separation of fracture surfaces occurred near the right end. Gradual decrease in oxidation from the left end to the right end of the fracture surfaces reveals the path followed by fracture. Absence of surface oxides in the final separation zone on the right side (Fig. 24a, B) may be due to the fact that after the separation of fracture surfaces this area was exposed to air at high temperature for a relatively shorter time period.

Figure 25 gives typical macro- and microfractographs from 19-9DL alloy creep-rupture specimen exposed at 870°C and 41 MPa stress level. Figure 25a (A and B) shows macrofractographic views of the mating fractured surfaces. In general, the fracture surfaces appeared very rough and heavily oxidized due to exposure to air at a higher temperature (870°C). Figure 25b shows the side view of the fracture surface in Fig. 25a (B). Many surface cracks are visible. This fracture also started at multiple locations at the outer surfaces. The separation of the fractured surfaces seemed to have progressed from the left end of the specimen to the right, because the

ORIGINAL PAGE IS
OF POOR QUALITY

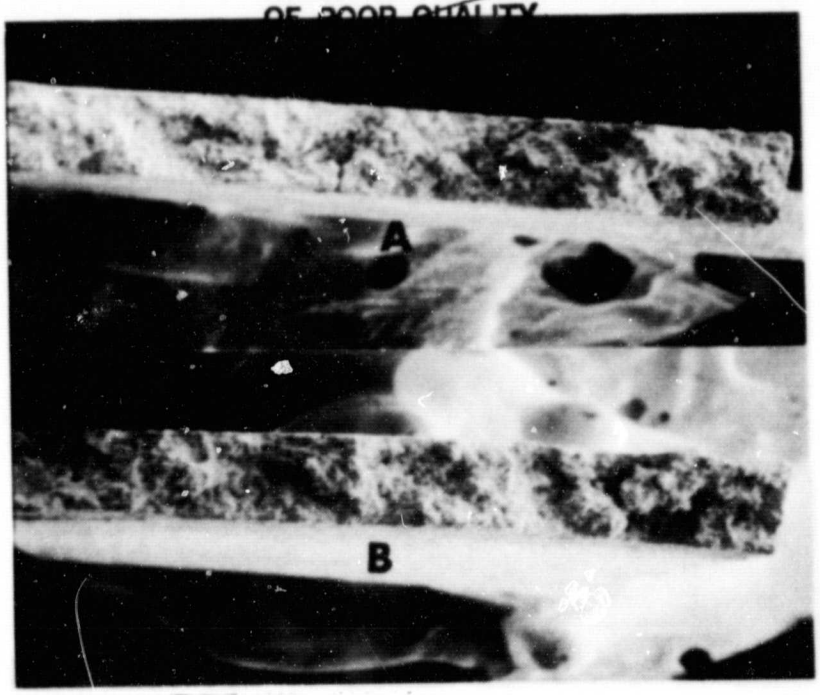

SEM No. 6486, 6487 ~15X

(a)

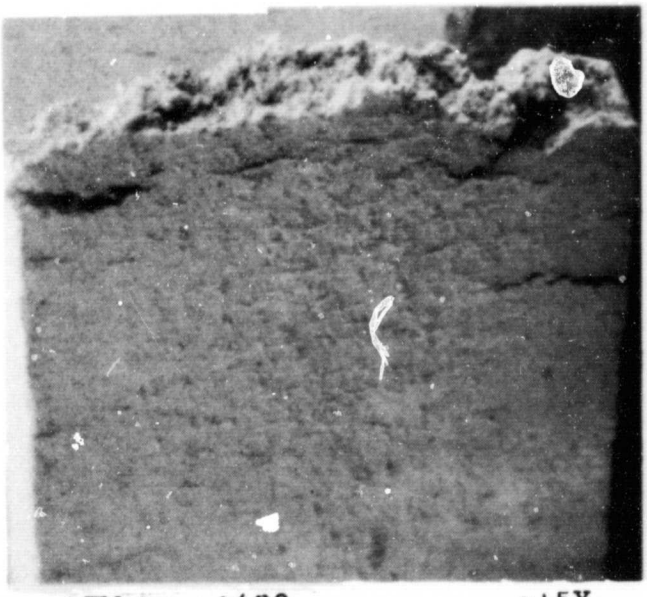

SEM No. 6492 ~15X

(b)

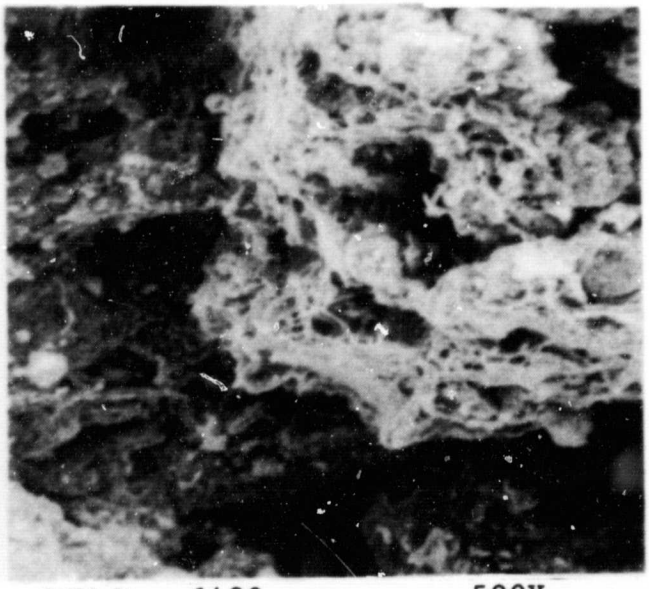

SEM No. 6490 500X

(c)

Figure 25

Typical Macro- and Microfractographs of the 19-9DL Specimen Creep Rupture Tested at 870°C and 41 MPa. (a) Macrofractographs of the mating fracture surfaces; (b) side view of fracture surface in Fig. 25a (B); and (c) microfractograph from the center of fracture surface in Fig. 25a (B).

fracture appeared increasingly rougher toward the right due to overload. Figure 25c shows a typical microfractograph from the center of the specimen on surface B (Fig. 25a). Again, dimple rupture is the main mode of fracture. Figure 25c also shows a thick granular oxide layer covering nearly the entire area.

In the case of cast alloy XF-818, fracture analysis was performed on two creep rupture tested specimens: (1) 815°C, 138 MPa, and (2) 870°C, 97 MPa. In both cases, fractures were found to have very rough and jagged texture.

Figures 26a and b show low-magnification SEM macrofractographs of the mating fracture surfaces from XF-818 alloy specimen tested at 815°C and 138 MPa. This fracture apparently initiated at the edge of the specimen, areas a and b of Fig. 26a, where the fracture was relatively smoother and fine textured. The entire fracture displayed a jagged topography, and the areas c and d (Fig. 26a) were rough in appearance. The final separation occurred near the center of the specimen. Figure 26c shows a side view of the fracture surface shown in Fig. 26a. Many surface cracks which could act as initiation sites are clearly visible. In the initiation regions (areas a and b, Fig. 26a), the primary mode of fracture was dimple rupture (Fig. 26d). Figure 26d shows an area exhibiting a layer of fractured dendrites. The entire fracture surface was oxidized, especially areas c and d (Fig. 26a) where oxidation masked the entire fracture area. Figure 26e shows a microfractograph from the heavily oxidized area at the center of the specimen where the final separation seemed to have occurred.

In the XF-818 specimen that was creep rupture tested at 870°C and 97 MPa, the general appearance of the fracture was very similar to that of the 815°C specimen described above. Figures 27a and b show the overall macrofractographic views of the mating fracture surfaces from the 870°C specimen. The entire fracture consisted of jagged faces of which areas a, c,

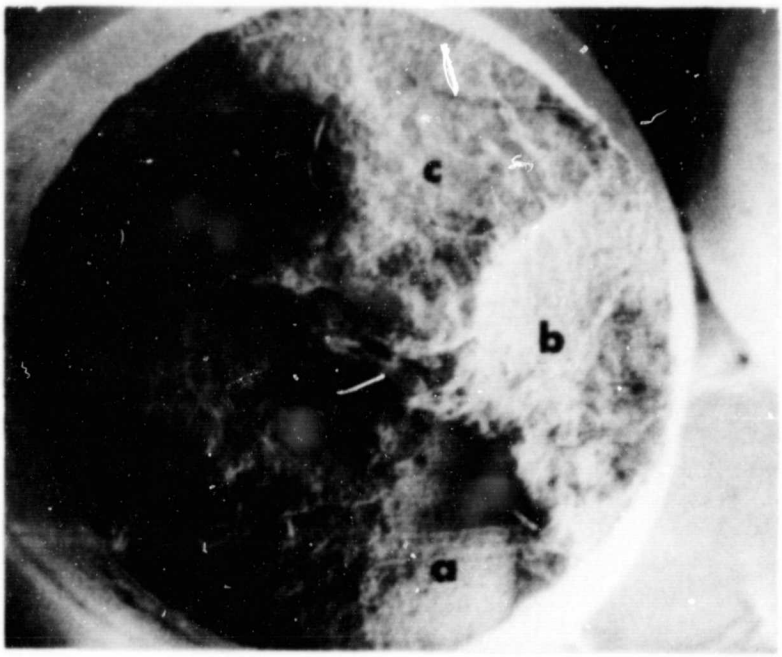

SEM No. 6494 ~20X

(a)

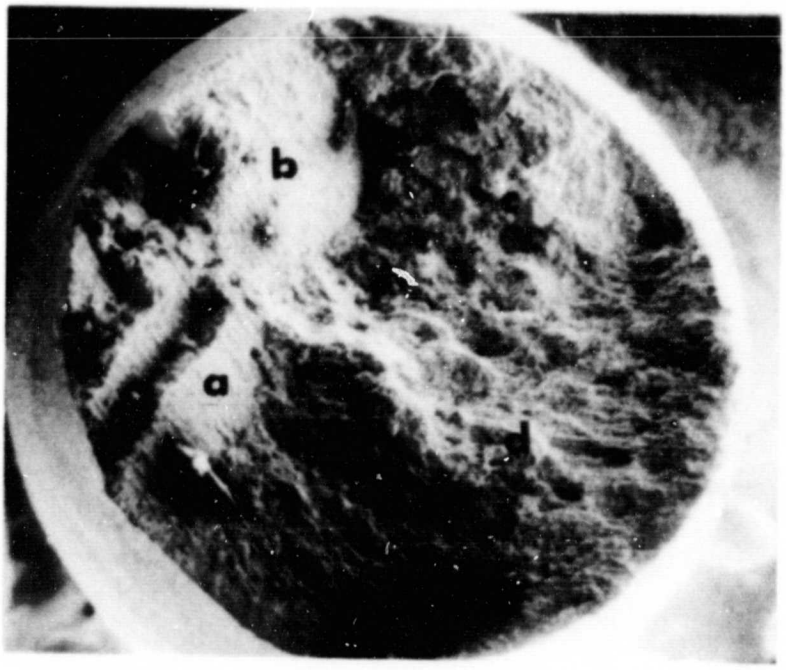

SEM No. 6493 ~20X

(b)

Figure 26

Typical Macro- and Microfractographs of XF-818 Specimen Creep Rupture Tested at 815°C and 138 MPa. (a,b) Macrofractographs showing corresponding areas of mating fracture surfaces; (c) side view of fracture surface in (a); microfractographs from (a): (d) area a and (e) overload region in center.

SEM No. 6500B ~20X

(c)

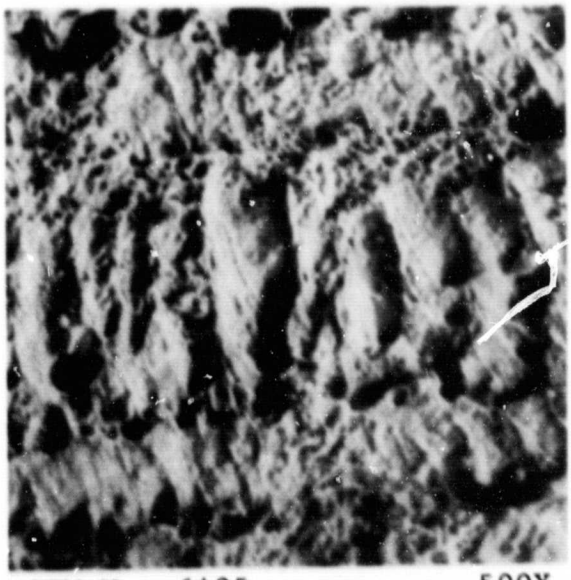

SEM No. 6495 500X

(d)

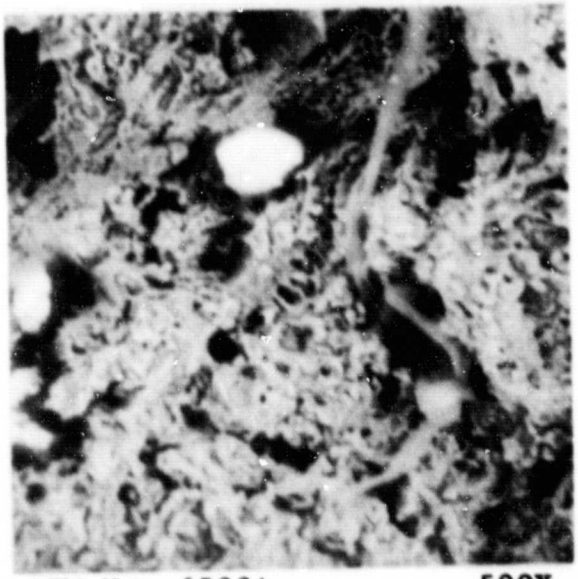

SEM No. 6500A 500X

(e)

Figure 26 (cont.)

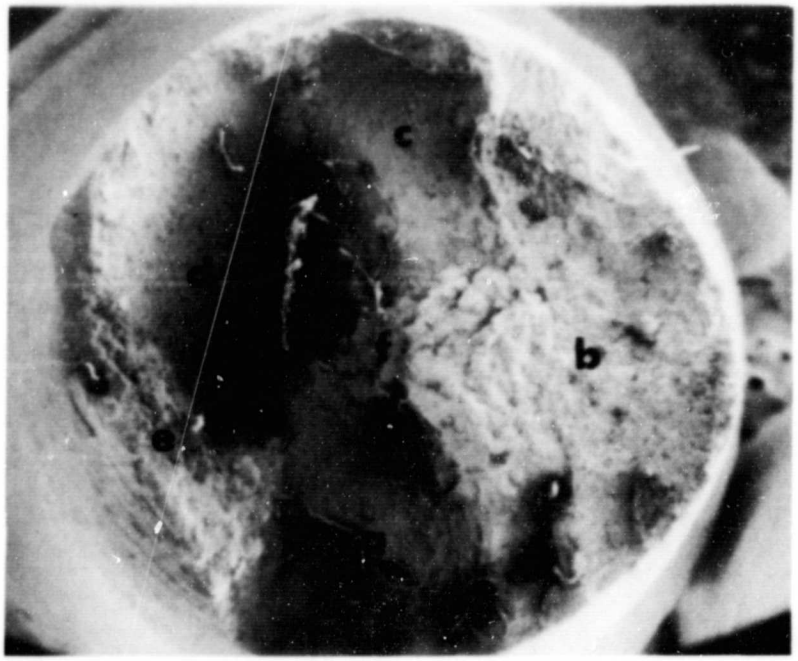

ORIGINAL PAGE IS
OF POOR QUALITY

SEM No. 6501 ~20X

(a)

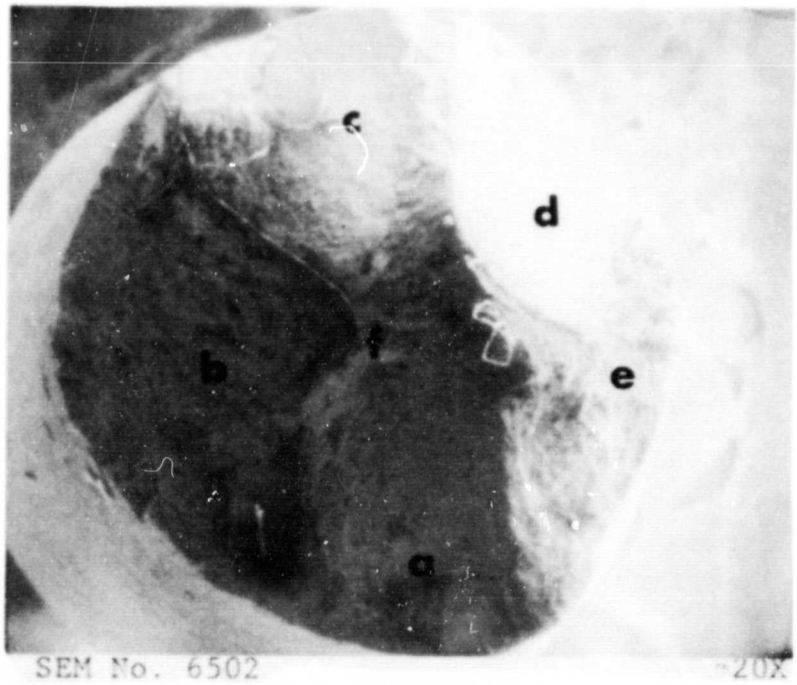

SEM No. 6502 ~20X

(b)

Figure 27

Typical Macro- and Microfractographs of XF-818 Specimen Creep Rupture Tested at 870°C and 124 MPa. (a,b) Macrofractographs of mating fracture surfaces showing corresponding areas; and microfractographs from areas in (a): (c) area a, (d) area b, and (e) overload zone, area f.

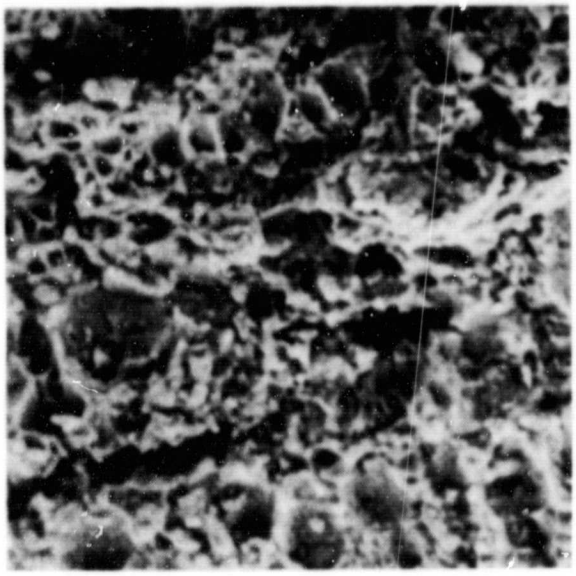

SEM No. 6502B 500X

(c)

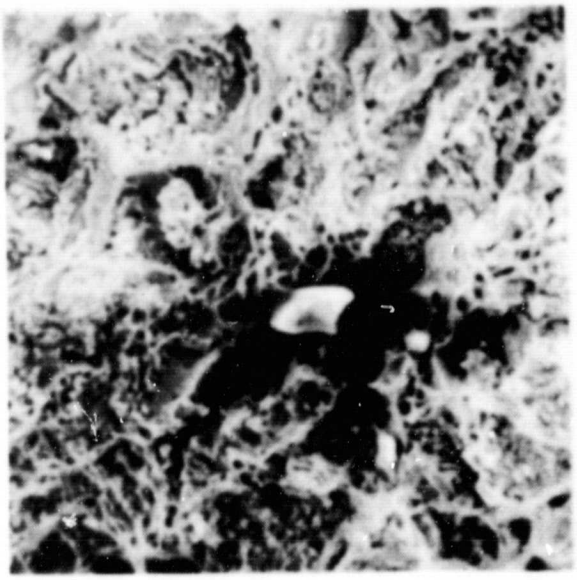

SEM No. 6503 500X

(d)

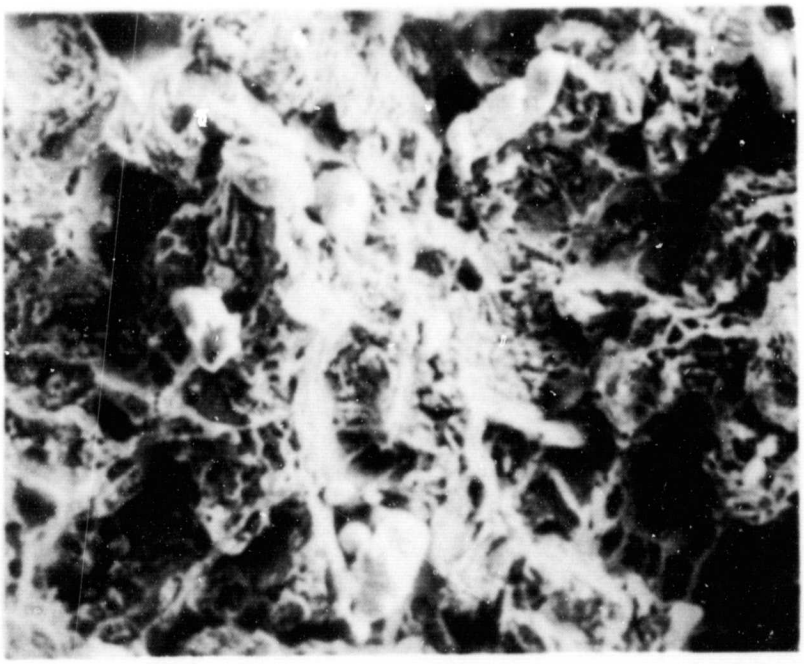

SEM No. 6504 500X

(e)

Figure 27 (cont.)

and appeared relatively smoother than areas b, e, and f. The fracture initiation zone could not be clearly identified, but it seemed that this fracture may have initiated at multiple locations near the edge of the specimen and progressed along smoother areas. The rougher areas indicate the regions which separated later under overload. Figures 27c and d show typical microfractographs from areas a and b, respectively (Fig. 27a). Area a (Fig. 27c) fracture has a smoother appearance, but the finer fracture features are masked by surface oxides. Area b (Fig. 27d) clearly shows evidence of fracture by dimple rupture mode. The fracture appearance in areas c and d (Fig. 27a) was similar to that shown in Fig. 27c. Fracture features observed in area e were very similar to those of area b (Fig. 27d). In area f, which represented final separation under overload, fracture occurred mainly by dimple rupture mode (Fig. 27e). In general, the 870°C specimen showed more surface oxidation that the 815°C specimen of the same alloy.

2.4 Task IV - Hydrogen Charging

All the NASA specimens were hydrogen-charged at 760°C, 100 hr at 20.7 MPa pressure. These specimens were immediately sent to NASA.

2.5 Task V - Reporting Requirements

The monthly reports for October (IITRI-M6061-13) and November (IITRI-M6061-14) were sent on time.

A project review meeting is planned for January 12, 1981 at IITRI where the current status of the program will be reviewed.

3. FUTURE WORK

During the next quarter, all air tests are expected to be completed.

The high-pressure creep-rupture facility will under go a thorough shakedown trial, temperature profile calibration, and extensometer evaluation. On completion of successful trials, short-term tests will be initiated during the quarter.

APPENDIX A

CREEP-RUPTUPE DATA IN AIR

Table A-1

BASIC CREEP-RUPTURE DATA FOR A286 TESTED IN AIR

Test Temp. °F	Test Temp. °C	Stress ksi	Stress MPa	Rupture Life, hr	Min. Creep Rate, sec^{-1}	Total Elong., %
1200	650	70	483	36.2	5.56 E-07	11.4
		60	414	568.1	3.03 E-09	8.4
		45 }a	310	1047+	9.72 E-11	0.38+
		90 }	620	1048	-	9.8
1300	705	55	379	35.0	1.25 E-07	13.8
		40	276	706.6	1.89 E-09	21.0
		34	234	1222	1.22 E-10	3.4
		26 }a	179	923.3+	1.53 E-10	0.27+
		75 }	517	924.1	-	19.8
1400	760	50	345	5.4	5.56 E-06	26.3
		40	276	27.2	2.06 E-07	25.9
		26	179	254.8	5.56 E-09	18.0
		18	124	1181	1.21 E-10	8.7
		12 }a	83	923.3+	2.39 E-10	0.27+
		60 }	414	924.1	-	18.5
1500	815	20	138	9.9	3.47 E-08	44.6
		16	110	89.7	3.45 E-08	25.4
		12	83	206.4	1.11 E-08	16.0
		9.0	62	439.5	6.42 E-09	11.8
		8.0	55	1030	2.29 E-08	10.7
		6.0 }a	41	867.1+	2.2 E-09	2.7
		40 }	276	868.4	-	24.2
1600	870	12	83	0.8	-	80.5
		8.0	55	15.0	1.06 E-05	59.2
		6.0	41	59.8	1.85 E-06	87.2
		3.0[b]	21	6222+	1.72 E-07	29.8+
1700	925	4.0	28	53.0	2.33 E-06	58.4
		3.0[b]	21	171.9	6.28 E-07	42.9
		2.5[b]	17	2214+	6.95 E-09	38.7+
		1.3[b]	9.0	552.4+	4.17 E-08	6.6+

[a] Uploaded to fracture

[b] Discontinued without failure

Table A-2

BASIC CREEP-RUPTURE DATA FOR INCOLOY 800H TESTED IN AIR

Test Temp. °F	Test Temp. °C	Stress ksi	Stress MPa	Rupture Life, hr	Min. Creep Rate, sec^{-1}	Total Elong., %
1200	650	40	276	54.8	2.64 E-07	32.2
		36	248	101.4	-	26.3
		30	207	309	6.94 E-08	15.0
		27 [a]	186	2078+	4.59 E-09	7.6+
1300	705	27	186	46.2	6.25 E-07	26.8
		18	124	848.1	3.61 E-08	36.8
		16	110	1475	2.28 E-08	19.6
1400	760	22	152	4.7	4.72 E-06	46.8
		18	124	28.9	1.71 E-06	53.0
		15	103	132.2	5.47 E-07	43.7
		11	76	1265	2.78 E-08	28.1
1500	815	16	110	14.6	4.44 E-06	59.6
		12,5	86	37.5	1.03 E-06	22.3
		12	83	72.6	-	32.1
		11	76	83.2	4.89 E-07	23.3
		9.0	62	780.6	1.74 E-08	18.1
		6.0 [b]	41	854.3+	1.36 E-09	0.70+
		15	103	858.3	-	26.0
1600	870	11	76	19.3	1.39 E-06	32.2
		9.0	62	39.3	4.81 E-07	15.9
		7.0	48	161.0	1.50 E-07	18.1
		4.5 [b]	31	868.4+	1.31 E-09	1.0
		11	76	873.8	-	32.3
1700	925	7.0	48	53.0	1.75 E-07	24.0
		6.0	41	130.5	5.50 E-08	23.2
		4.5	31	292.2	5.56 E-08	19.7
		3.0 [b]	21	710.3+	1.39 E-09	1.19+
		7.0	48	726.4	-	21.6

[a] Discontinued without failure

[b] Uploaded to fracture

Table A-3

BASIC CREEP-RUPTURE DATA FOR N-155 TESTED IN AIR

Test Temp. °F	Test Temp. °C	Stress ksi	Stress MPa	Rupture Life, hr	Min. Creep Rate, sec^{-1}	Total Elong., %
1200	650	60	414	2.7	4.63 E-06	23.6
		55	379	14.8	7.45 E-07	19.9
		40	276	968.7	2.78 E-08	26.2
1300	705	40	276	42.5	6.72 E-07	28.4
		28	193	527.8	6.11 E-08	46.0
1400	760	35	241	9.0	1.85 E-06	42.7
		28	193	36.8	1.25 E-06	44.0
		24	165	7.5[a]	-	-
		24	165	115.3	4.14 E-07	51.5
		18	124	573.6	5.00 E-08	30.1
1500	815	24	165	7.5	4.44 E-06	58.3
		18	124	42.5	1.50 E-06	53.2
		16	110	128.8	2.92 E-07	46.8
		12	83	457.3	5.28 E-08	25.0
		11	76	931.3	2.94 E-08	34.7
		9.1	63	2536	7.51 E-09	12.1
1600	870	16	110	8.9	6.67 E-06	65.0
		13.5	93	55.6	1.94 E-07	59.6
		12	83	58.0	9.92 E-07	46.9
		10	69	212.2	2.11 E-07	35.9
		8.5	59	636.7	5.56 E-08	26.7
1700	925	10	69	32.7	4.86 E-07	38.8
		8.5	59	49.2	1.07 E-06	43.3
		6.0	41	354.2	9.17 E-08	27.7

[a]Data rejected. Most likely a faulty specimen. Duplicate tested.

Table A-4

BASIC CREEP-RUPTURE DATA FOR 19-9DL TESTED IN AIR

Test Temp. °F	Test Temp. °C	Stress ksi	Stress MPa	Rupture Life, hr	Min. Creep Rate, sec^{-1}	Total Elong., %
1200	650	60	414	1.1	4.72 E-06	18.8
		40	276	135.9	3.58 E-08	11.9
1300	705	40	276	10.9	5.97 E-07	16.9
		25	172	268.5	5.69 E-08	24.2
		19	131	1342	1.14 E-08	12.1
1400	760	28	193	8.5	1.35 E-06	30.0
		25	172	20.2	6.95 E-07	31.0
		20	138	101.0	3.22 E-07	37.4
		14.5	100	739.1	1.86 E-08	18.8
		12.5	86	1687	5.77 E-09	12.1
1500	815	20	138	2.8	2.22 E-05	44.8
		18	124	14.2	3.33 E-06	33.4
		15	103	66.4	4.33 E-07	29.2
		12	83	173.1	1.44 E-07	32.3
		10.5	72	324.1	6.03 E-08	25.0
		8.6	59	1118	5.72 E-09	10.1
1600	870	15	103	1.8	1.89 E-05	61.6
		12	83	10.2	5.00 E-06	42.4
		10	69	38.0	1.60 E-06	36.4
		8.0	55	107.9	3.47 E-07	34.3
		6.0	41	406.3	3.19 E-08	20.8
		4.8	33	799.0	2.00 E-08	-
1700	925	10	69	4.1	1.58 E-05	47.6
		8.0	55	16.3	3.06 E-06	37.1
		5.0	35	177.2	1.25 E-07	27.5

Table A-5

BASIC CREEP-RUPTURE DATA FOR CRM-6D TESTED IN AIR

Test Temp. °F	Test Temp. °C	Stress ksi	Stress MPa	Rupture Life, hr	Min. Creep Rate, sec^{-1}	Total Elong., %
1200	650	65	448	0.1	-	1.3
		60	414	0.1	-	2.1
		55	379	305.0	1.82 E-08	4.2
1300	705	50	345	49.1	1.59 E-08	7.8
		45	310	147.4	1.06 E-07	8.6
		40	276	827.4	1.37 E-08	8.2
1400	760	42	290	11.5	1.01 E-06	7.9
		40	276	23.6	6.28 E-07	10.7
		35	241	140.2	8.61 E-08	9.9
		32	221	354.4	3.28 E-08	10.3
		30	207	796.7	9.03 E-09	8.7
		28[a]	193	470+	<3.91 E-09	1.9+
1500	815	35	241	7.1	1.16 E-06	13.9
		28	193	78.6	1.49 E-07	11.8
		25	172	281.9	2.86 E-08	10.6
		22	152	768.0	6.11 E-09	7.6
1600	870	22	152	29.7	2.94 E-07	11.7
		17	117	430.5	7.64 E-09	5.6
		17[b]	117	401.9	9.81 E-09	6.6
1700	925	17	117	28.4	1.79 E-07	12.5
		13	90	237.3	1.13 E-08	5.5

[a]Test terminated due to grip failure.

[b]Repeat test to check reproducibility.

Table A-6

BASIC CREEP-RUPTURE DATA FOR XF-818 TESTED IN AIR

Test Temp. °F	Test Temp. °C	Stress ksi	Stress MPa	Rupture Life, hr	Min. Creep Rate, sec^{-1}	Total Elong., %
1200	650	76	524	0.1	-	6.2
		72	496	0.1	-	5.4
		60	414	143.2	6.72 E-08	7.5
1300	705	60	414	3.1	1.60 E-06	6.7
		55	379	20.9	3.97 E-07	7.2
		48	331	103.0	9.42 E-08	10.1
1400	760	50	345	2.3	4.12 E-06	8.2
		38	262	38.4	3.50 E-07	12.7
		32	221	132.3	1.16 E-07	13.6
		30	207	261.7	5.67 E-08	12.7
		22	152	2497	4.58 E-09	11.4
1500	815	35	241	4.2	2.77 E-06	13.1
		25	172	62.5	3.50 E-07	22.3
		20	138	199.5	8.33 E-08	14.1
1600	870	25	172	4.1	5.15 E-06	16.9
		17	117	58.5	3.64 E-07	20.6
		14	97	194.0	9.00 E-08	19.0
		9.2	63	2198	6.78 E-09	12.9
1700	925	15	103	11.8	2.11 E-06	25.2
		10	69	128.5	1.46 E-07	23.1

Table A-7

HIGH-TEMPERATURE CREEP-RUPTURE DATA ON A-286 TESTED IN AIR

Test Temp., °C	Stress, MPa	Time to Rupture, hr	Total Elong., %	Time, hr To Reach Different Creep Elongations (%) 0.1	1.0	5.0	To Onset of Tertiary Creep
(1)	(2)	(3)	(4)	(5)	(6)	(7)	(8)
650	483	36.2	11.4	--	0.2	16.4	22.0
	414	568.1	8.4	93.0	380.0	530.0	260
705	379	35.0	13.8	0.7	13.0	26.2	7.0
	276	706.6	21.8	220.0	542.0	648.0	460
	234	1222.0	3.3	770.0	1095	--	600
760	345	5.4	26.3	--	0.3	2.3	--
	276	27.2	25.9	0.2	10.5	21.3	7.0
	179	254.8	18.0	60.0	156	208.0	110
	124	1181.0	7.2	240	500	950.0	250
815	138	9.9	44.6	1.8	8.1	--	6.0
	110	89.7	25.4	6.0	27.5	48.0	20.0
	83	206.4	16.0	32.0	70.0	135.0	40.0
	62	439.5	11.8	62.0	162.0	338.0	90.0
	55	1030	10.7	83.0	234.0	--	--
870	83	0.8	80.5	--	--	0.3	--
	55	15.0	59.2	--	0.3	1.3	5.0
	41	59.8	87.2	0.3	1.5	7.2	30.0
	21	6222+	29.8	1.2	19.5	80.0	4500
925	28	53.0	58.4	0.1	1.0	5.0	30.0
	21	171.9	42.9	0.4	3.5	17.5	140.0
	17	2214	38.7	0.7	7.0	34.0	--
	9.0	552.4	--	1.5	70.0	336	--

Table A-8

HIGH-TEMPERATURE CREEP-RUPTURE DATA ON INCOLOY 800H TESTED IN AIR

Test Temp., °C	Stress, MPa	Time to Rupture, hr	Total Elong., %	Time, hr To Reach Different Creep Elongations (%) 0.1	1.0	5.0	To Onset of Tertiary Creep
(1)	(2)	(3)	(4)	(5)	(6)	(7)	(8)
650	276	54.8	32.2	0.1	3.0	31.0	19.0
	248	101.4	26.3				
	207	309	15.0	0.1	8.7	150.0	120
	186	2078	7.6	0.6	63.0	1730	1100
705	186	46.2	26.8	--	1.0	17.5	16.0
	124	848.1	36.8	0.7	50.0	335	275
	110	1475	15.5	0.2	25.0	450	400
760	152	4.7	46.8	--	0.4	2.5	2.0
	124	28.9	53.0	--	0.5	6.7	6.0
	103	132.2	43.7	0.2	3.0	20.0	70.0
	76	1265	28.1	0.7	68.0	466.0	475.0
815	110	14.6	59.6	--	0.2	2.0	4.0
	86	37.5	22.3	0.1	1.8	12.8	13.5
	83	72.6	32.1				
	76	83.2	23.3	0.1	4.5	27.5	40.0
	62	780.6	18.1	--	78.0	437.0	250.0
870	76	19.3	32.2	0.1	2.1	8.1	4.5
	62	39.3	15.9	0.3	5.5	23.4	12.0
	48	161.0	18.1	0.8	19.0	78.0	44.0
925	48	53.0	24.0	1.0	14.0	31.0	11.0
	41	131.0	23.2	4.0	38.5	75.0	22.0
	31	292.2	19.7	3.0	48.0	149	62.0

Table A-9

HIGH-TEMPERATURE CREEP-RUPTURE DATA ON N-155 TESTED IN AIR

Test Temp., °C	Stress, MPa	Time to Rupture, hr	Total Elong., %	Time, hr: To Reach Different Creep Elongations (%) 0.1	1.0	5.0	Time, hr: To Onset of Tertiary Creep
(1)	(2)	(3)	(4)	(5)	(6)	(7)	(8)
650	414	2.7	23.6	--	0.5	--	0.75
	379	15.0	19.9	--	1.7	--	13.0
	276	968.7	26.2	0.4	20.0	315	475
705	276	42.5	28.4	--	0.8	15.0	20.0
	193	527.8	46.0	0.8	16.0	185	200
760	241	9.0	42.7	--	0.2	1.8	--
	193	36.8	44.0	--	1.0	9.8	12.0
	165	115.3	51.5	0.5	4.0	31.0	50.0
	124	573.6	30.1	0.8	16.0	213	290
815	165	7.5	58.3	--	0.2	1.4	--
	124	42.5	53.2	0.2	1.3	8.8	20.0
	110	129.0	46.8	0.2	3.0	38.0	50.0
	83	457.3	25.0	0.7	19.0	200	180
	76	931.3	34.7	1.5	30.0	370	325
	63	2536	--	1.6	170	1440	1800
870	110	8.9	65.0	--	0.2	1.9	2.1
	93	56.0	59.6	0.3	12.0	28.0	11.0
	83	58.0	46.9	0.1	2.5	14.0	24.0
	69	212.2	35.9	0.3	7.0	60.0	83.0
	59	636.7	26.7	0.4	29.0	226	220
925	69	33.0	38.8	0.2	5.0	17.5	8.5
	59	49.2	43.3	0.1	2.0	12.0	16.0
	41	354.2	27.7	1.0	29.0	143	120

Table A-10

HIGH-TEMPERATURE CREEP-RUPTURE DATA on 19-9DL TESTED IN AIR

Test Temp., °C	Stress, MPa	Time to Rupture, hr	Total Elong., %	Time, hr To Reach Different Creep Elongations (%) 0.1	1.0	5.0	To Onset of Tertiary Creep
(1)	(2)	(3)	(4)	(5)	(6)	(7)	(8)
650	414	1.1	18.8	--	0.6	--	0.6
	276	135.9	11.9	--	32.0	133.0	55.0
705	276	10.9	16.9	--	0.7	--	--
	172	268.5	24.2	2.0	50.0	158.0	65.0
	131	1342	12.1	10.0	152.0	950	650.0
760	193	8.5	30.0	--	0.2	--	--
	172	20.2	31.0	--	2.5	15.5	14.5
	138	101.0	37.4	0.1	9.0	41.5	34.0
	100	739.1	18.8	2.0	89.0	497.0	280.0
	86	1687.0	10.9	5.0	300	1250	425
815	138	2.8	44.8	--	0.1	0.6	1.9
	124	14.2	33.4	--	0.4	3.2	11.0
	103	66.4	29.2	0.1	4.0	27.5	22.0
	83	173.1	32.3	--	11.0	82.0	62.0
	72	324.1	25.0	0.4	40.0	190.0	105.0
	59	1118.0	9.4	1.7	30.0	900	350
870	103	1.8	61.6	--	--	0.6	0.5
	83	10.2	42.4	--	0.4	2.5	3.2
	69	38.0	36.4	--	1.2	8.2	17.0
	55	107.9	34.3	0.1	8.0	39.5	45.0
	41	406.3	20.8	2.0	82.0	260.0	130.0
	33	799.0	--	1.5	89.0	440.0	290.0
925	69	4.1	47.6	--	0.2	0.9	1.8
	55	16.3	37.1	--	0.7	4.2	4.5
	35	177.2	27.5	0.1	10.5	81.0	55.0

Table A-11

HIGH-TEMPERATURE CREEP-RUPTURE DATA ON CRM-6D TESTED IN AIR

Test Temp., °C	Stress, MPa	Time to Rupture, hr	Total Elong., %	Time, hr: To Reach Different Creep Elongations (%) 0.1	1.0	5.0	Time, hr: To Onset of Tertiary Creep
(1)	(2)	(3)	(4)	(5)	(6)	(7)	(8)
650	448	0.1	1.3	--	--	--	--
	414	0.1	2.1	--	--	--	--
	379	305.0	4.2	0.1	36.0	--	180.0
705	345	49.1	7.8	--	6.0	44.5	20.0
	310	147.4	8.6	--	12.0	108.0	70.0
	276	827.4	8.2	0.2	53.0	700.0	475.0
760	290	11.5	7.9	--	1.6	--	6.5
	276	23.6	10.7	--	2.9	18.4	14.0
	241	140.2	9.9	0.2	12.0	115.0	80.0
	221	354.4	10.3	0.2	20.0	298.0	240.0
	207	796.7	8.7	0.5	59.0	770.0	610.0
815	241	7.1	13.9	--	0.6	6.3	4.2
	193	78.6	11.8	--	6.5	63.5	40.0
	172	281.9	10.6	0.2	19.0	252.0	175.0
	152	768.0	7.6	0.3	58.0	760.0	440.0
870	152	29.7	11.7	0.3	6.0	28.0	17.0
	117	430.5	5.6	0.3	80.0	--	230.0
	117	401.9	6.6	0.4	125.0	401.0	215.0
925	117	28.4	12.5	0.2	8.5	26.3	12.0
	90	237.3	5.5	0.4	146.0	--	130.0

Table A-12

HIGH-TEMPERATURE CREEP-RUPTURE DATA ON XF-818 TESTED IN AIR

Test Temp., °C	Stress, MPa	Time to Rupture, hr	Total Elong., %	Time, hr To Reach Different Creep Elongations (%) 0.1	1.0	5.0	To Onset of Tertiary Creep
(1)	(2)	(3)	(4)	(5)	(6)	(7)	(8)
650	524	0.1	6.2	--	--	--	--
	496	0.1	5.4	--	--	--	--
	414	143.2	7.5	0.1	11.0	--	100.0
705	414	3.1	6.7	--	0.3	--	--
	379	20.9	7.2	--	3.5	--	11.0
	331	103.0	10.1	0.1	10.5	83.5	50.0
760	345	2.3	8.2	--	0.3	--	--
	262	38.4	12.7	--	4.5	28.0	17.0
	221	132.3	13.6	0.1	14.0	92.0	50.0
	207	261.7	12.7	0.3	31.5	184.0	80.0
	152	2497	11.4	2.0	300	1930	860.0
815	241	4.2	13.1	--	0.5	--	3.3
	172	62.5	22.3	0.2	5.0	32.0	24.0
	138	199.5	14.1	0.2	14.5	135.0	95.0
870	172	4.1	16.9	--	0.4	2.3	1.9
	117	58.5	20.6	0.1	4.5	31.0	22.0
	97	194.0	19.0	0.1	14.0	117.0	65.0
	63	2198	12.9	3.5	205.0	1420	640.0
925	103	11.8	25.2	--	0.8	5.8	5.0
	69	128.5	23.1	0.3	15.0	71.0	42.0

APPENDIX B

STATISTICAL ANALYSIS OF ALLOY 19-9DL DATA

Table B-1

STATISTICAL ANALYSIS OF ALLOY 19-9 DL LIFE DATA

1. TEMPERATURE-COMPENSATED ANALYSIS OF LIFE:

$$\ln t = \ln k_2 + n_2 \ln \sigma + \frac{Q_2}{RT} \qquad (1)$$

WHERE

t = TIME TO RUPTURE (t_r), HR

= TIME TO REACH 1% STRAIN ($t_{0.01}$), HR

= TIME TO TERTIARY CREEP (t_{ter}), HR

σ = APPLIED STRESS, MPA

T = TEST TEMPERATURE, °K

Q_2 = ACTIVATION ENERGY OF CREEP-RUPTURE PROCESS kJ/°K-GMOLE

n_2 = STRESS EXPONENT

k_2 = CONSTANT.

Table B-1 (cont.)

2. THE RUPTURE LIFE (t_r) DATA ARE ANALYZED IN FOUR DIFFERENT WAYS WITH THE FOLLOWING RESTRICTIONS ON STRESS AND LIFE:

   A) NO RESTRICTION, ALL DATA, 25 NOS.
   B) STRESS RESTRICTION ONLY, σ < 276 MPA, 22 NOS.
   C) LIFE RESTRICTION ONLY, t_r > 3.6 E-02 MS (10 HR), 20 NOS.
   D) BOTH STRESS AND LIFE RESTRICTION, σ < 276 MPA, t_r > 3.6 E-02 MS, 18 NOS.

3. REARRANGE EQUATION 1 AS FOLLOWS:

$$\ln \sigma = \frac{1}{n_2} \left(\ln t - \frac{Q_2}{RT} \right) - \frac{\ln k_2}{n_2}$$

PLOT $\ln \sigma$ VS. $\left(\ln t_r - \frac{Q_2}{RT} \right)$ AND

FIT REGRESSION LINE TO IT FOR EACH ONE OF THE FOUR DATA SUBSETS.

Table B-2

STATISTICAL ANALYSIS OF ALLOY 19-9 DL MINIMUM CREEP RATE DATA

1. TEMPERATURE-COMPENSATED ANALYSIS OF MINIMUM CREEP RATE ($\dot{\varepsilon}_m$).

$$\ln \dot{\varepsilon}_m = \ln k_1 + n_1 \ln \sigma + \frac{Q_1}{RT} \qquad (2)$$

WHERE Q_1 = ACTIVATION ENERGY FOR SECONDARY CREEP PROCESS.

ANALYSES FOR THE FOUR SUBSETS OF THE DATA.

2. REARRANGE EQUATION 2 AS FOLLOWS:

$$\ln \sigma = \frac{1}{n_1} \left(\ln \dot{\varepsilon}_m - \frac{Q_1}{RT} \right) - \frac{\ln k_1}{n_1}$$

AND PLOT $\ln \sigma$ VS. $\left(\ln \dot{\varepsilon}_m - \frac{Q_1}{RT} \right)$ AND FIT REGRESSION LINE TO IT FOR EACH OF THE FOUR DATA SUBSETS.

APPENDIX C

Table C-1

STATISTICAL ANALYSIS OF N-155 AND XF-818 ALLOY DATA

1. TEMPERATURE-COMPENSATED ANALYSIS OF LIFE:

$$\ln t = \ln k_2 + n_2 \ln \sigma + \frac{Q_2}{RT} \qquad (1)$$

2. RUPTURE LIFE (t_r) DATA ARE ANALYZED IN FOUR DIFFERENT WAYS WITH THE FOLLOWING RESTRICTIONS ON STRESS AND LIFE:

RESTRICTION	XF-818		N-155	
	LEVEL	NO. OF DATA	LEVEL	NO. OF DATA
1. NONE	-	18	-	24
2. STRESS, MPA (KSI)	<483 (70)	16	<379 (55)	22
3. LIFE, MS (HR)	>3.6 E-02 (10)	14	>3.6 E-02 (10)	20
4. STRESS (MPA), AND LIFE (MS)	<483 (70), >3.6 E-02 (10)	13	<379 (55), >3.6 E-02 (10)	19